NAVAL POSTGRADUATE SCHOOL

MONTEREY, CALIFORNIA

THESIS

A LOW-FIDELITY SIMULATION TO EXAMINE THE DESIGN SPACE FOR AN EXPENDABLE ACTIVE DECOY

by

Devon A. Cartwright

December 2017

Thesis Advisor:	Alejandro Hernandez
Co-Advisor:	Oleg Yakimenko
Second Reader:	Brian Connett

THIS PAGE INTENTIONALLY LEFT BLANK

REPORT DOCUMENTATION PAGE			*Form Approved OMB No. 0704–0188*
Public reporting burden for this collection of information is estimated to average 1 hour per response, including the time for reviewing instruction, searching existing data sources, gathering and maintaining the data needed, and completing and reviewing the collection of information. Send comments regarding this burden estimate or any other aspect of this collection of information, including suggestions for reducing this burden, to Washington headquarters Services, Directorate for Information Operations and Reports, 1215 Jefferson Davis Highway, Suite 1204, Arlington, VA 22202-4302, and to the Office of Management and Budget, Paperwork Reduction Project (0704-0188) Washington, DC 20503.			
1. AGENCY USE ONLY ***(Leave blank)***	**2. REPORT DATE** December 2017	**3. REPORT TYPE AND DATES COVERED** Master's thesis	
4. TITLE AND SUBTITLE A LOW-FIDELITY SIMULATION TO EXAMINE THE DESIGN SPACE FOR AN EXPENDABLE ACTIVE DECOY		**5. FUNDING NUMBERS**	
6. AUTHOR(S) Devon A. Cartwright			
7. PERFORMING ORGANIZATION NAME(S) AND ADDRESS(ES) Naval Postgraduate School Monterey, CA 93943-5000		**8. PERFORMING ORGANIZATION REPORT NUMBER**	
9. SPONSORING /MONITORING AGENCY NAME(S) AND ADDRESS(ES) N/A		**10. SPONSORING / MONITORING AGENCY REPORT NUMBER**	
11. SUPPLEMENTARY NOTES The views expressed in this thesis are those of the author and do not reflect the official policy or position of the Department of Defense or the U.S. Government. IRB number ____N/A____.			
12a. DISTRIBUTION / AVAILABILITY STATEMENT Approved for public release. Distribution is unlimited.		**12b. DISTRIBUTION CODE**	

13. ABSTRACT (maximum 200 words)

A new type of expendable radar decoy, one that leverages the advances in technology of the last 50 years, is required to improve the survivability of non-stealth aircraft against radar-guided threats. This thesis applies modeling and simulation based systems engineering to explore the design space of a notional active expendable decoy to determine the combination of key performance parameters that will maximize probability of survival. The thesis focuses on development of a Microsoft Excel-based simulator, which accepts inputs from the user, uses a nearly orthogonal Latin hypercube experimental design, and performs multiple simulator runs with stochastic model variables. The final output includes statistical analysis of results to provide the user with the best combination of design variables to improve survivability against specified threat parameters. Results show that either low power with high gain, or high power with low gain, was the best combination for maximizing probability of survival. In addition, low altitude deployments are to be avoided unless the missile is very near the target aircraft. The results provided by the tool are notional, based on realistic approximations of radar, aircraft, and decoy systems. The results will inform the acquisition strategy of NAVAIR.

14. SUBJECT TERMS expendable active decoy, EAD, radar countermeasures, modeling and simulation based systems engineering, MSBSE			**15. NUMBER OF PAGES** 99
			16. PRICE CODE
17. SECURITY CLASSIFICATION OF REPORT Unclassified	**18. SECURITY CLASSIFICATION OF THIS PAGE** Unclassified	**19. SECURITY CLASSIFICATION OF ABSTRACT** Unclassified	**20. LIMITATION OF ABSTRACT** UU

NSN 7540–01-280-5500 Standard Form 298 (Rev. 2–89)
Prescribed by ANSI Std. 239–18

THIS PAGE INTENTIONALLY LEFT BLANK

Approved for public release. Distribution is unlimited.

A LOW-FIDELITY SIMULATION TO EXAMINE THE DESIGN SPACE FOR AN EXPENDABLE ACTIVE DECOY

Devon A. Cartwright
Lieutenant, United States Navy
B.S., University of Kansas, 2009

Submitted in partial fulfillment of the
requirements for the degree of

MASTER OF SCIENCE IN SYSTEMS ENGINEERING

from the

NAVAL POSTGRADUATE SCHOOL
December 2017

Approved by: Alejandro Hernandez
Thesis Advisor

Oleg Yakimenko
Co-Advisor

CDR Brian Connett
Second Reader

Ronald Giachetti
Chair, Department of Systems Engineering

THIS PAGE INTENTIONALLY LEFT BLANK

ABSTRACT

A new type of expendable radar decoy, one that leverages the advances in technology of the last 50 years, is required to improve the survivability of non-stealth aircraft against radar-guided threats. This thesis applies modeling and simulation based systems engineering to explore the design space of a notional active expendable decoy to determine the combination of key performance parameters that will maximize probability of survival. The thesis focuses on development of a Microsoft Excel-based simulator, which accepts inputs from the user, uses a nearly orthogonal Latin hypercube experimental design, and performs multiple simulator runs with stochastic model variables. The final output includes statistical analysis of results to provide the user with the best combination of design variables to improve survivability against specified threat parameters. Results show that either low power with high gain or high power with low gain was the best combination for maximizing probability of survival. In addition, low altitude deployments are to be avoided unless the missile is very near the target aircraft. The results provided by the tool are notional, based on realistic approximations of radar, aircraft, and decoy systems. The results will inform the acquisition strategy of NAVAIR.

THIS PAGE INTENTIONALLY LEFT BLANK

TABLE OF CONTENTS

LIST OF FIGURES

LIST OF TABLES

THIS PAGE INTENTIONALLY LEFT BLANK

LIST OF ACRONYMS AND ABBREVIATIONS

ASPD	Advanced Self Protection Decoys
C2	command and control
CEADS	Cartwright Expendable Active Decoy Simulator
CNR	carrier-to-noise ratio
DOE	design of experiments
DRFM	digital radio frequency memory
DOD	Department of Defense
EAD	expendable active decoy
ECM	electronic countermeasure
EM	electromagnetic
ESAMS	Enhanced Surface-to-Air Missile Simulation
EW	early warning, electronic warfare
GEN-X	Generic Expendable
J/S	jam-to-signal ratio
KRET	Radioelectronic Technologies Concern
LO	low observable
M&S	modeling and simulation
MBSE	model based systems engineering
MOE	measure of effectiveness
MSBSE	modeling and simulation based systems engineering
MTS	multi-spectral targeting system
NAVAIR	Naval Air Systems Command
NOLH	nearly orthogonal Latin hypercube
RCS	radar cross section
ROC	receiver operating characteristics
SE	systems engineering
SOI	system of interest

THIS PAGE INTENTIONALLY LEFT BLANK

EXECUTIVE SUMMARY

Currently fielded expendable countermeasure systems cannot adequately protect friendly aircraft from modern radar-guided threats. The primary method of radar countermeasures employed on most aircraft is chaff technology, but other methods include towed decoys and/or electronic jamming. Unfortunately, each of these methods has shortcomings such as high cost, feasibility issues, and capability limitations. Chaff is inexpensive and may be used on nearly all aircraft but has a limited capability. Towed decoys are very capable systems, but they have limited numbers of decoys, relatively high cost, and their employment is not feasible on all aircraft. Electronic jamming is similarly capable as towed decoys, but it is not feasible to have a dedicated jamming platform for every mission or to fit the electronics on every airframe. Developing a new type of countermeasure that combines the best characteristics of each method with fewer limitations is possible with today's technology.

Developing an Expendable Active Decoy (EAD) can leverage evolving technologies from the last five decades. An EAD is a system that when launched, samples the electromagnetic (EM) spectrum broadcast by a radar, records the signal, applies phase and frequency shifts to the recording, and then rebroadcasts the signal in order to mislead the enemy radar. The radar-guided threat will then steer toward a false target that appears in a different location.

Other countries have already developed EAD systems, such as the BriteCloud system created by Selex ES (now Leonardo) of the UK, Advanced Self Protection Decoys (ASPD) created by Reut Systems & Technologies of Israel, and the President-S system developed by Radioelectronic Technologies Concern (KRET) of Russia. The EAD systems fit into the physical space occupied by traditional chaff cartridges and are expended much the same way. However, with the EAD's onboard digital radio frequency memory (DRFM) technology, it can sample the electromagnetic spectrum produced by a threat radar, record the signal, and replay it with a stronger return than the target aircraft. This process enables an EAD to capture a missile signal in its terminal phase and "walk" it off the target.

One of the benefits of attempting to design an EAD, versus a new type of chaff, is that one removes the difficulty of modeling a complex chaff cloud and instead models the dynamics of a single object. This simplifies the modeling process so that a low-fidelity discrete event simulation may be able to predict the performance parameters of the system of interest (SOI) accurately. The systems engineering process utilizes the low-fidelity simulation developed in this thesis during the early phases of the systems acquisition process: namely, the concept exploration, concept of operations, and system requirements phases. This low-fidelity simulation allows designers and engineers to explore the design space of the SOI and to perform an analysis of alternatives to provide high-level system requirements. Therefore, using this simulation now to ensure rapid acquisition of a desperately needed capability is important.

Initial modeling was conducted utilizing Microsoft Excel to act as a validation tool for the simulation that would eventually be developed. The author reviewed a thesis written by Jeremy Braud in 2014 at NPS that examined the possibility of using Microsoft Office products, namely Excel, to create an Electronic Attack Route Optimization tool to validate the potential of using non-compiled software to develop military specific applications (Braud 2014). The findings of his thesis showed that Microsoft Office software provided a means for constructing useful modeling and simulation tools. This convinced the author that the capabilities of pre-approved software installed on Department of Defense (DOD) computers would be the preferred method for development of the simulation. Additionally, the wide proliferation of Microsoft Excel ensures that users of the simulation will require minimal training in order to maximize the simulator's utility.

To employ a modeling and simulation based systems engineering approach requires development of an acceptable model. The computer simulation scenario uses an open-ocean engagement of a friendly helicopter by an enemy surface vessel. An open-ocean engagement removes the possibility of terrain masking from the friendly helicopter's repertoire of defensive tactics. This thesis supports an EAD system in development by NAVAIR, which will be used on naval aircraft in the maritime environment. Additionally, open-ocean reduces the possibility of multi-path effects playing a role and simplifies their calculation when they do occur.

The scenario employs the MH-60S helicopter because it is the most predominant U.S. Navy rotary-wing aircraft and fulfills the anti-surface warfare mission set. Additionally, the inherent speed and maneuverability limitations of the airframe preclude the possibility of out maneuvering or out running the threat missile. Lastly, this aircraft represents the worst-case scenario in terms of radar cross section (RCS) of naval aircraft because of complex interactions of the airframe and rotor systems. If an EAD is capable of decoying a radar-guided threat when employed from a helicopter, then logically the effectiveness should improve when employed from a fighter or transport aircraft that has greater maneuverability and speed.

The frequency range of interest for this thesis is from 2 – 18 Ghz. To validate the simulation later in the study, the threat radar chosen was the Castor 2 J/C radar shown in Figure 8. It operates within the frequency range of interest and is a commonly used fire control radar on foreign naval vessels. The missile systems paired with the Castor 2 J/C are semi-active guided systems. According to a one-on-one interaction with Dr. Robert Harney (2017), bistatic radars best represent semi-active guided systems with the radar being the transmitter and the missile being the receiver. According to Streetly's *Jane's Radar and Electronic Warfare Systems 2005–2006*, the Castor 2 J/C radar is a broadband, J-band, monopulse-Doppler tracking radar. It has a peak power of 30 kilowatts, a maximum range of 30 km, and a tracking accuracy of 5 m. It also incorporates an EO/IR suite for passive tracking and target acquisition (Streetly 2006).

The Cartwright Expendable Active Decoy Simulator (CEADS) is the result of the integration of all of the models into a single simulator. Each of the aforementioned models is integrated into the Excel-based simulation on individual tabs. A tab exists to represent the EAD, radar, missile, multipath, and sea surface clutter models. The models are cross-linked so that if a shared value changes on one tab, it changes on all corresponding models that use the same value.

CEADS accepts input from the user on the radar, missile, aircraft, EAD, and environment variables. The performance parameters of the missile, aircraft, EAD, environment, and Castor 2 J/C radar are input into the associated models. The radar, missile, and EAD models calculate the CNR of the aircraft as seen by the radar or missile

and compare them to the required CNR for a specified detection probability. The EAD model goes further by also calculating the CNR generated by the EAD given the EAD performance parameters input by the user. The result is either non-detection of the aircraft due to the CNR being below the detection threshold, aircraft detection because the CNR is above the threshold or aircraft non-detection because the EAD CNR causes a jam-to-signal ratio of greater than one.

The simulation allows a systems engineer to examine the key measure of effectiveness (MOE) for the EAD system. These key MOEs drive the value of a new system to the stakeholder and drive the requirements that the systems engineer will set for the system. The key MOE for this simulator focuses on whether or not the EAD can successfully drive the missile to a geometry that it is no longer able to engage the aircraft. This happens when the J/S produced by the EAD is significant enough that the missile remains focused on the EAD as it falls away from the aircraft until the missile's range and altitude no longer permit it to receive the radar returns off the target. At this point, the MOE declares the simulator run a success and moves on to the next run. If the EAD fails to decoy the incoming missile, then the missile's focus will remain on the target aircraft and will eventually strike the target resulting in a failure.

The factors that the author believes will have the greatest outcome on the success of the EAD are those factors that are inherent to the system. These factors are the variables contained in Equations 8 and 9 for jam-to-signal ratio. Those factors are EAD transmitter power, EAD loss factor, EAD gain, EAD bandwidth, and EAD deployment range. Other factors that the author believes to be significant, but are not necessarily captured in any equations, are EAD vertical and horizontal accelerations, and EAD vertical and horizontal velocities. These factors will have an effect on how long the EAD remains airborne and how quickly it can drive the missile to an unfavorable geometry. These ten factors shown combine to create the design of experiments (DOE) for CEADS.

Sequential experimentation enables the researcher to focus on the most relevant areas of the design space. As such, a screening experiment first identifies the most relevant factors that affect the MOE, as well as significant interactions among the factors. The next set of experiments incorporates a nearly orthogonal Latin hypercube (NOLH) design. A

NOLH allows for efficient exploration of the system design space and provides a good amount of information about the experimental region. NOLH also allows for simplified analysis of results though regression analysis and similar methods. This study examines 10 factors that the researcher believes or is uncertain about the influence on the MOE. The design of experiments used for this thesis is an 11 x 33 NOLH from Cioppa (2002). Each design point is unique in its combination of values, and constitutes a singular instantiation of a potential EAD design.

CEADS uses the NOLH DOE to test many possible combinations of the EAD design space against an individual radar and missile system. This allows for analysis of the data in order to determine the best combination of performance parameters that maximizes the EAD effectiveness against a particular threat. Testing the CEADS against the Castor 2J/C radar will prove the simulator is a useful tool. Beyond the scope of this thesis, CEADS allows for data collection for a multitude of threat systems, analysis of data, and aides in developing high-level system requirements.

The data that resulted from the sensitivity analysis demonstrates that CEADS produces statistically relevant results. The author collected the results of the sensitivity analysis and sorted them to show which combinations of variables produced the highest probability of success. The data shows that either a low power setting with a high gain, or a high power with a low gain, is necessary to achieve high probability of success. None of 10–100-watts design points succeeded in achieving a probability of success of 90%. Design Point 3 had the most instances of 90% or greater probability of success. These results will be crucial to the development of system level requirements for a future EAD.

References

Braud, Jeremy J. 2014. “Electronic Attack Platform Placement Optimization.” Master’s thesis, Naval Postgraduate School. https://calhoun.nps.edu/handle/10945/43881

Cioppa, Thomas M. 2002. “Efficient Nearly Orthogonal and Space-Filling Experimental Designs for High-Dimensional Complex Models.” PhD Diss. Naval Postgraduate School. https://calhoun.nps.edu/handle/10945/9808

Harney, Robert C. 2017. *Discussion on Radar Model Characteristics*, edited by Devon A. Cartwright.

Streetly, Martin. 2005. *Jane's Radar and Electronic Warfare Systems 2005-2006*. Jane's Information Group Limited. pp. 160-161

ACKNOWLEDGMENTS

I would like to thank my advisors, Professor Alejandro Hernandez and Professor Oleg Yakimenko. Your mentorship and guidance helped make sure that my thesis was of top quality. I also thank my second reader, Commander Brian Connett. Our one-on-one sessions helped me put things in perspective when I was struggling with certain concepts. You always had good insight and were a solid sounding board.

I would also like to thank my beautiful wife, Audrey, for supporting me through all of the hard times. Her love and devotion made it easier to shoulder the burdens of the difficult days and appreciate the easy ones. I want to thank my amazing daughter, Everleigh. Watching her learn and grow in the first seven months of her life encourages me to never stop learning.

THIS PAGE INTENTIONALLY LEFT BLANK

I. INTRODUCTION

The introduction chapter provides an overview of methods currently employed to protect aircraft from radar-guided threats. The author compares these methods, and shortcomings are noted to identify a problem statement: Currently fielded expendable countermeasure systems cannot adequately protect friendly aircraft from modern radar-guided threats. Lastly, the author provides a summary of the thesis organization.

A. BACKGROUND

In the age of stealth aircraft eluding detection, destroying their targets, and returning to base, some may consider the idea of expendable radar countermeasures to be antiquated; however, the author does not believe so. Only a few aircraft have ever implemented a full suite of what is known as low observable (LO) technology. Fighter aircraft such as the F-22 Raptor and F-35 Lightning II, and bombers such as the B-2 Spirit and F-117 Nighthawk have radar cross sections the size of a bird or smaller (Yue 2001). While LO technology protects them from a large number of threats, they are not impervious to detection. In 1999, an F-117 was shot down over Kosovo by an SA-3 infrared guided missile. In 2001, a British defense firm known as Roke Manor developed a prototype method of detecting stealth aircraft utilizing currently installed cellphone antenna infrastructure to act as a type of multi-static radar (Yue 2001). As recently as November 2016, *Popular Mechanics* magazine reported that China claims that its newest radars demonstrated the capability to detect America's stealthiest aircraft, the F-22 Raptor (Mizokami 2016). With the recent demonstrations of America's most survivable aircraft being detectable, even they can benefit from countermeasures. Additionally, because most other aircraft in the military's inventory are not LO, a method of protecting them from missile engagement is still necessary. The primary method of radar countermeasures employed on most aircraft is chaff technology, but other methods include towed decoys and/or electronic jamming. Unfortunately, each of these methods has shortcomings such as high cost, feasibility issues, and capability limitations.

Towed decoys, such as the Raytheon AN/ALE-50 employed on non-LO fighter aircraft, restrict the ability to maneuver and require a very specific missile-aircraft orientation to be effective. Additionally, the aircraft can only carry a very limited number of single-use towed decoys. Figure 1 shows a towed decoy deployed behind a fighter aircraft.

Helicopters do not employ towed decoys because of the possibility of the line entanglement in the main or tail rotor. Transport and other non-fighter aircraft do not employ towed decoys because they do not operate in threat environments that require radar-guided threat defense. Unfortunately, the missile engagement zones of many radar-guided threats are constantly expanding, which will likely put these aircraft in range. In a recent interview, Neil Ashdown, deputy editor of *IHS Jane's Intelligence Review* stated that the Chinese HQ-9 system, a derivative of the Russian S-300, has a 230 km range (Ashdown 2016). This could put American command and control (C2), early warning (EW), and refueling aircraft at risk.

While aircraft can use towed decoys effectively to protect themselves, currently no system exists to retrieve a decoy if it has been deployed but not used. At present, if a decoy is deployed, the aircraft must cut the fiber optic cable to release it prior to landing. *Defense Industry Daily* states that the price of a single decoy is $22,000 and has a 10-year shelf life. The loss of a towed expendable each time it is deployed and the limited shelf life are shortcomings that can be overcome.

Figure 1. Towed Decoy behind Eurofighter Typhoon. Source: Onnis (2012).

Electronic jamming is an active measure that can be effective at defending against radar-guided threats; however, due to the sophistication of integrated electronic systems involved, jamming often requires a separate dedicated platform. Such jamming is infeasible for helicopters and other aircraft, because such aircraft cannot fit the electronic systems in their already space-constrained airframes.

Since jamming is an "active" measure, it is possible for a radar operator to determine that the radar is experiencing jamming indicating the presence of a threat. The operator may tune the radar system to the situation to overcome the jamming or to alert other radar systems to the presence of the threat. Tactically, remaining undetected to the radar as long as possible and responding only if detection occurs is the best strategy. Aircraft with limited electronic warfare (EW) or electronic countermeasure (ECM) capabilities require an on demand expendable system to remain undetected while also retaining the capability to defeat a threat if encountered.

Chaff is a passive expendable countermeasure that provides an on demand defense against radar-guided threats. Chaff consists of millions of fibers that are about the thickness of a human hair and only a few centimeters or less in length. These fibers, known as dipoles, are typically aluminum coated fiberglass filaments cut to a specific length in order to have the greatest effect against a predetermined radar frequency. This restricts chaff effectiveness to a small number of threats that emit the wavelength corresponding to the length of the chaff dipoles.

Chaff works by deploying a canister full of chaff fibers into the moving airstream around an aircraft of ship. Much like blowing on a dandelion, the air moving past the vehicle causes the millions of dipoles to spread out into a large cloud within a few seconds. This cloud absorbs and re-transmits the incident radar energy to cause a radar return. If the radar dipoles are of the appropriate length for the radar system, the return that an operator sees on their display from the chaff cloud may be greater in magnitude than the return of the actual vehicle.

To create a chaff countermeasure that is useful against a broad range of radar frequencies, multiple dipole lengths per expendable canister, or multiple expendables with different length dipoles is required. The limited space on the aircraft and standard expendable canister sizes limits the total number of chaff dipoles carried in a single expendable canister. The Navy's primary chaff expendable RR-129A/AL, shown in the bottom of Figure 2, follows the first method and has three different dipole lengths corresponding to specific frequencies. Radars that do not transmit in those specific frequencies will likely be unaffected by the chaff. Additionally, chaff is less effective against modern threat radars that rely on Doppler and moving target indicator, as the chaff cloud will remain essentially stationary when compared to the target. The other chaff shown at the top of Figure 2 is RR-144A/AL, which is a training chaff that does not affect civilian air traffic control radars. The see through canisters are to show the internal arrangement of the chaff. The cluster of dipoles on the right side of the image shows the fibers separated from the canister.

U.S. Navy RR-144A/AL training chaff is shown on top and RR-129A/AL Chaff shown on bottom. Notice the different length in the RR-129A/AL compared to the uniform lengths in the RR-144A/AL. The fibers on the right show the dipoles outside of the canister.

Figure 2. Two Types of U.S. Navy Chaff. Source: Wikipedia (2008).

B. THE PROBLEM

Currently fielded expendable countermeasure systems cannot adequately protect friendly aircraft from modern radar-guided threats. Each of the aforementioned methods of radar countermeasures has drawbacks in capability, cost, or feasibility. Chaff is inexpensive and may be used on nearly all aircraft but has a limited capability. Towed decoys are very capable systems but they have limited numbers of decoys, relatively high cost, and their employment is not feasible on all aircraft. Electronic jamming is similarly capable as towed decoys but it is not feasible to have a dedicated jamming platform for every mission or to fit the electronics on every airframe. Developing a new type of

countermeasure that combines the best characteristics of each method with fewer limitations is possible with today's technology.

Chaff has been the primary expendable countermeasure used since World War II as a method of fooling enemy radar. However, with the advent of LO technologies, the United States halted its countermeasure research and redirected funding into this technology, which promised to make aircraft nearly invisible to radar. According to NAVAIR's Advanced Tactical Aircraft Protection Systems (PMA-272), there has been minimal research in the area of countermeasures since the 1970s (Koppenberger 2017). The chaff designs developed from this limited research are still the primary expendable radar decoys employed by all the U.S. military services nearly 50 years later. This chaff was designed to deal with early Cold War Soviet threats and while countermeasure research diminished, radar technology continued to improve.

A cursory search identifies few countermeasure research papers scattered throughout the decades since the 1970s. Of those papers, many cite the problems of accurately modeling a chaff cloud as the largest hurdle to overcome. (Knott et al. 1981) Research exists characterizing individual chaff cloud dipoles; however, it is difficult to model accurately the random nature of millions of individual dipole elements in differing environmental conditions without better fluid flow dynamic models (Scholfield et al. 2011).

Developing an Expendable Active Decoy (EAD) can leverage evolving technologies from the last five decades. An EAD is a system that when launched, samples the electromagnetic (EM) spectrum broadcast by a radar, records the signal, applies phase and frequency shifts to the recording, and then rebroadcasts the signal in order to mislead the enemy radar. The radar-guided threat will then steer toward a false target that appears in a different location. Figure 3 provides an example of what a radar operator might see in a range-Doppler map.

One of the benefits of attempting to design an EAD, vice a new type of chaff, is that one removes the difficulty of modeling a complex chaff cloud and instead models the dynamics of a single object. This simplifies the modeling process so that a low-fidelity

discrete event simulation may be able to predict the performance parameters of the system of interest (SOI) accurately.

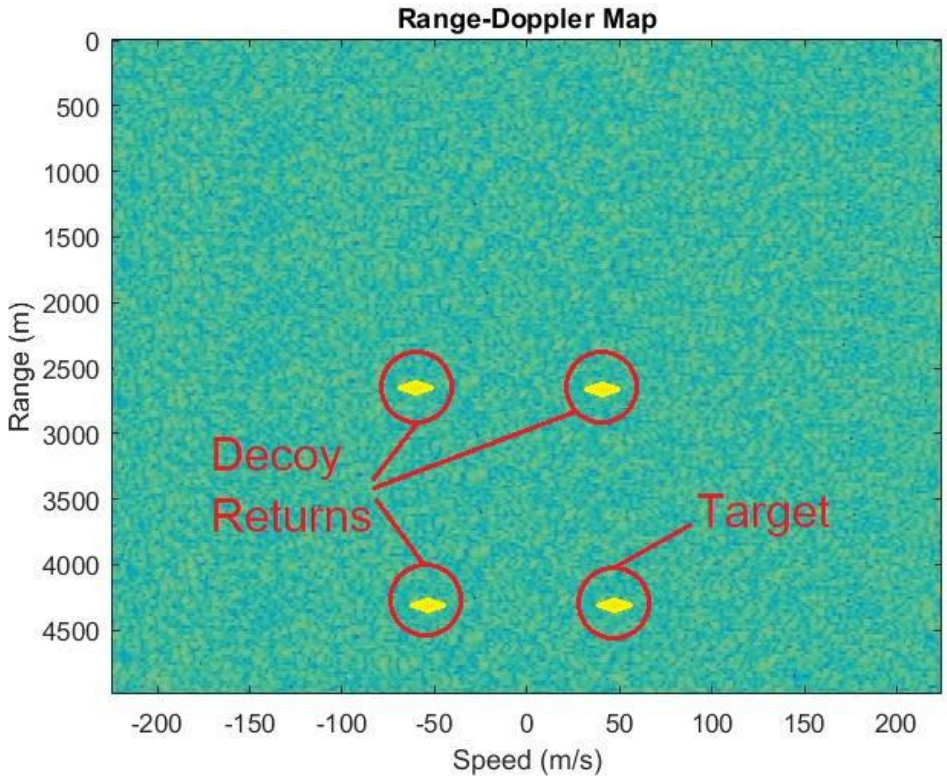

Figure 3. Example of Radar Returns from an Expendable Active Decoy

C. THESIS ORGANIZATION

The remainder of this thesis is organized as follows: Chapter II introduces the experiences and steps in the research process that led to the development of the thesis. Chapter III covers the development of the models that represent the various systems and environment and the integration of those models into the simulator. Chapter IV describes the Excel-based simulation developed during the project and provides an overview of its use case, and Chapter V presents the data obtained from running an example of the simulation and analysis/interpretation of those results. Lastly, Chapter VI presents the conclusion and recommendations.

THIS PAGE INTENTIONALLY LEFT BLANK

II. LITERATURE REVIEW

The author's tactical training to employ the MH-60S helicopter piqued an interest in radar-guided threats and countermeasures. Methods employed to defend against radar-guided threats have limited effectiveness because of the pilots' lack of understanding of the threats as well as the capabilities of the countermeasures. This judgement was validated when, while deployed in the Pacific theater, a non-allied ship engaged the author's aircraft with a targeting radar. The author's experience showed that the onboard countermeasures were likely ineffective against the targeting radar. The non-allied ship turned off the radar but, had the engagement progressed, the outcome would have been unfavorable for the aircraft. After arriving at Naval Postgraduate School, these judgements led the author to reach out to Naval Air Systems Command (NAVAIR) to determine whether it saw any value in continued countermeasure research. While this thesis does not aim to improve the understanding of the threats by the operator, the thesis addresses the capabilities of the countermeasures.

Meeting with representatives from NAVAIR made clear to the author that minimal research had been completed in the realm of radar countermeasures but the U.S. Navy determined that this was an issue that required attention. The author attended a survivability symposium in March of 2017 that brought together groups from various industries, educational institutions, and each military branch. One of the more promising methods presented to fill this capability gap was the development of an EAD system.

A. CURRENT EAD RESEARCH

Other countries have already developed EAD systems such as the BriteCloud system created by Selex ES (now Leonardo) of the UK, Advanced Self Protection Decoys (ASPD) created by Reut Systems & Technologies of Israel, and the President-S system developed by Radioelectronic Technologies Concern (KRET) of Russia. Figure 4 shows examples of these systems. The EAD systems fit into the physical space occupied by traditional chaff cartridges and are expended much the same way. However, with the EAD's onboard DRFM technology, it can sample the electromagnetic spectrum produced

by a threat radar, record the signal, and replay it with a stronger return than the target aircraft. This process enables an EAD to capture a missile signal in its terminal phase and "walk" it off the target.

The President-S Disposable Jamming Transmitter is shown on the left. The BriteCloud Expendable Active Decoy is shown on the right. The BriteCloud EAD is enlarged to show detail.

Figure 4. Expendable Active Decoy Systems Fielded by Russia and the UK. Sources: Kuzmin (2009); Chuter (2016).

The U.S. Navy, in cooperation with Raytheon and Texas Instruments, developed the RT-1489/ALE Generic Expendable (GEN-X) in the early 1990s; however, the production line no longer exists. The GEN-X is a basic EAD with a limited frequency range. At the symposium, PMA-272 stated that one of the primary concerns with developing a new EAD system is to avoid the same mistakes encountered in the GEN-X program, specifically, the battery and storage life problems. Besides improving the capability of the new EAD system to work across a broader frequency spectrum, it will be important to address the storage life concern. The battery storage-life concern is beyond the scope of this thesis. Figure 5 is an image of the GEN-X decoy.

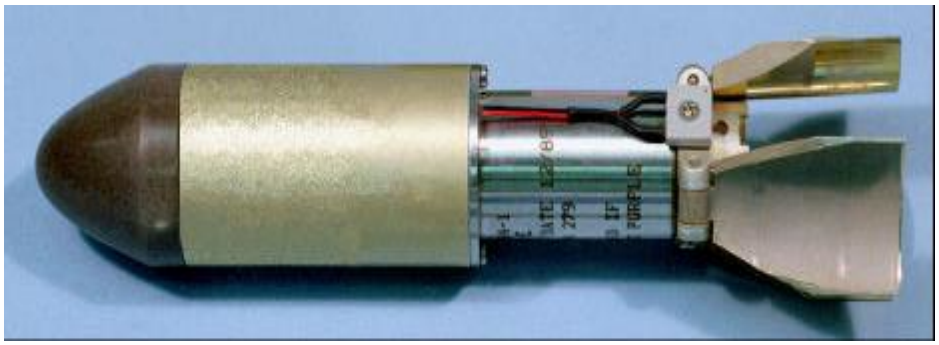

Figure 5. Prototype RT-1489/ALE GEN-X Decoy and Canister. Source: Koppenberger (2017).

B. COMPUTER SIMULATIONS FOR ANALYSIS

Computer programs presented at the symposium simulated engagements of aircraft by radar-guided threats. One of the limitations discussed was outdated programming languages utilized to create the simulations, making it difficult to update. The simulations were also unreliable and required a large amount of computing power along with specialized training to execute. One of the more useful software programs presented was the Enhanced Surface-to-Air Missile Simulation (ESAMS). ESAMS takes multiple models, developed over the last several decades, and combines them into a single simulation to leverage the capabilities of each, creating an in depth simulation tool. Figure 6 shows the input models for ESAMS.

While this simulation is an extremely powerful tool, it represents a very high-fidelity model that is better used in the later stages of the systems engineering (SE) process that can be used to verify earlier SE efforts. This experience convinced the author that a low-fidelity simulation is necessary to replicate the ESAMS results earlier in the SE process. This replication effort will require less computing power, minimal training to operate, and can retain appropriate classification levels for the environment in which it is exercised.

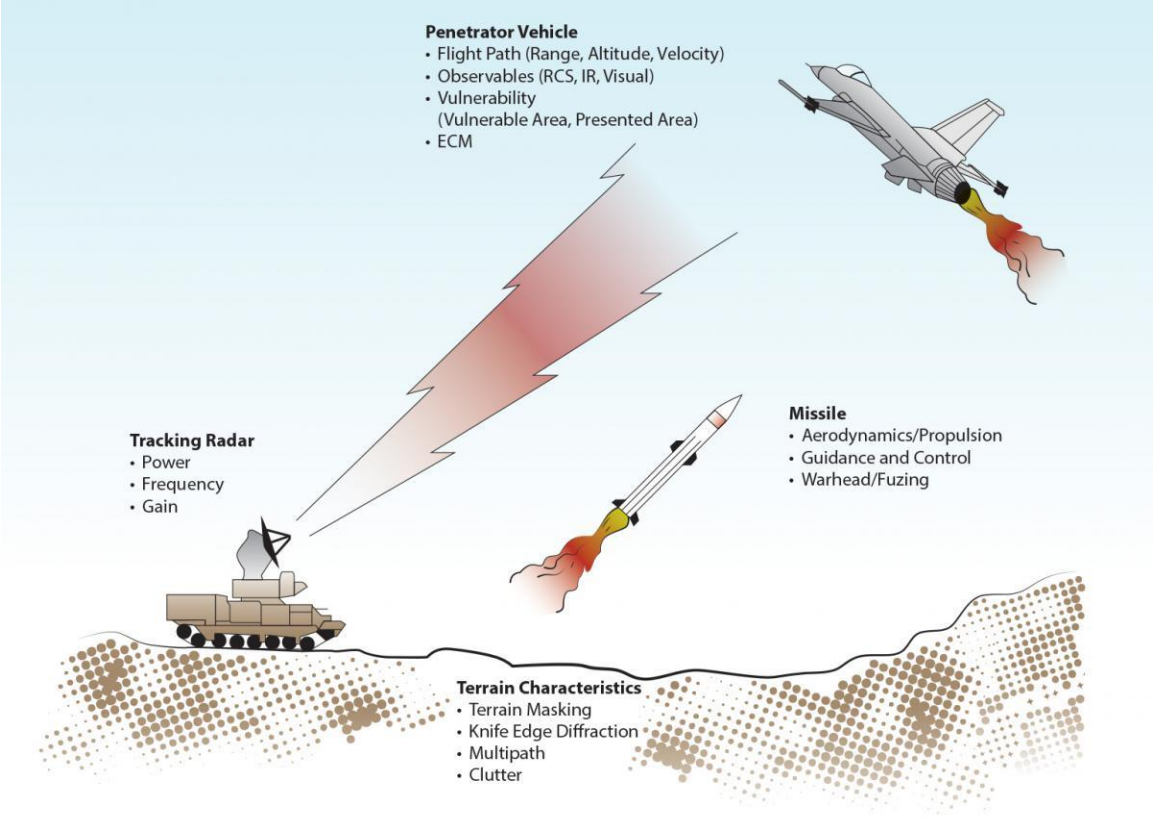

Figure 6. ESAMS Model Elements. Source: Defense Systems Information Analysis Center (2017).

C. BENEFITS OF MODELING AND SIMULATION IN THE SYSTEM ENGINEERING PROCESS

According to the *INCOSE Systems Engineering Handbook*, the benefits of modeling and simulation (M&S) in the SE process include confirming of system requirements and behavior prior to development and proving insight and clarification to designers and engineers to minimize errors while maximizing productivity. This helps to reduce cost and schedule overruns by obtaining information about the system early in the design process and prior to major commitment of resources. The data that results from M&S provides data to the analyst, supports decision-making, and informs stakeholders of the outcome of their preferences as well as system limitations and capabilities. Additionally, the models provide a common framework for engineers that aid in developing a shared understanding of the system requirements.

The systems engineering process utilizes the low-fidelity simulation developed in this thesis during the early phases of the systems acquisition process: namely, the concept exploration, concept of operations, and system requirements phases as shown in Figure 7. This low-fidelity simulation allows designers and engineers to explore the design space of the SOI and to perform an analysis of alternatives to provide high-level system requirements. According to Benjamin Blanchard and Wolter Fabrycky, systems engineering efforts undertaken early in the system acquisition process can result in cost savings, reduced acquisition times, and a reduction in risks. All of these combine to ensure stakeholder satisfaction with the final product (Blanchard and Fabrycky 2006, 48). Therefore, using this simulation now to ensure rapid acquisition of a desperately needed capability is important.

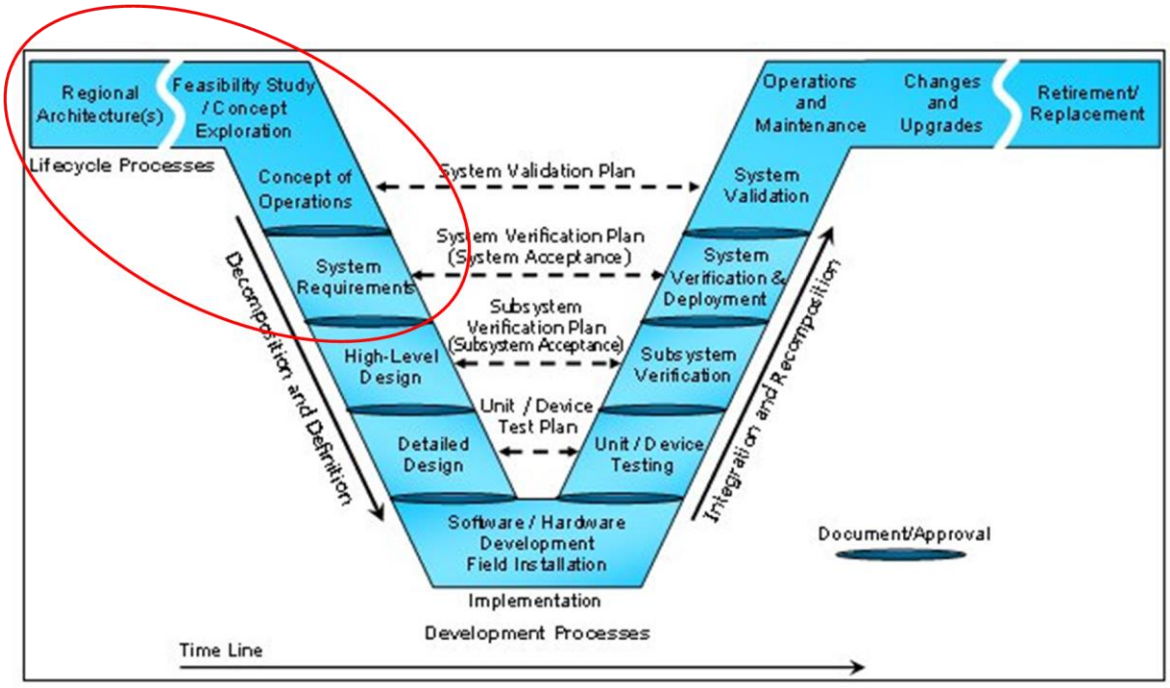

Figure 7. Systems Engineering Process "V" Model.
Adapted from Rausch et al. (2007).

As recently as October of 2017 at the National Defense Industrial Association's Systems Engineering Conference, the commander of NAVAIR Vice Admiral Paul Grosklags communicated that NAVAIR requires a new model-based systems engineering

environment that solves integration and training problems, and reduces the time to design, test, and evaluate new systems. The current process involves giving 500-page specification documents to industry, asking them to interpret the requirements, and build a system from scratch. This practice hinders the ability to make little changes along the way, while testing changes in a virtual environment allows for rapid solution generation. With accurate information from stakeholders, it is possible to build a computer model, insert notional aircraft or weapons systems, and provide the model to industry to facilitate system design. The intent is also to use the models as verification tools later in the SE process to assess program maturation and to validate earlier assumptions. He added that the benefits of model-based systems engineering extend throughout test and evaluation, production, and sustainment phases and can demonstrate system robustness over the system life cycle. NAVAIR plans to implement model-based systems engineering into any future program to provide the opportunity to learn as quickly as possible and to achieve the benefits previously listed. Working in direct contact with NAVAIR, this thesis and the resulting models and simulation directly support the vice admiral's call to action (Eckstein 2017).

D. PRIMARY MODEL REFERENCES

Modeling the individual elements of the simulation, requires a deeper review of physics and equation-based approximations inherent in the engineering of the radar, missile, aircraft, and EAD systems. For this, the author turned to the writings of Dr. Robert Harney of the Naval Postgraduate School and Dr. Graham Brooker of the University of Sydney Australian Centre for Field Robotics. The aforementioned authors' publications provide the necessary mathematical models to represent the tracking radar, multipath, clutter, aircraft, and EAD system. Physics-based models were adapted from the author's operational knowledge to model the flight paths of the missile, aircraft, and EAD.

Initial modeling was conducted utilizing Microsoft Excel to act as a validation tool for the simulation that would eventually be developed. The author reviewed a thesis written by Jeremy Braud in 2014 at NPS that examined the possibility of using Microsoft Office products, namely Excel, to create an Electronic Attack Route Optimization tool to validate the potential of using non-compiled software to develop military specific applications

(Braud 2014). The findings of his thesis showed that Microsoft Office software provided a means for constructing useful modeling and simulation tools. This convinced the author that the capabilities of pre-approved software installed on Department of Defense (DOD) computers would be the preferred method for development of the simulation. Additionally, the wide proliferation of Microsoft Excel ensures that users of the simulation will require minimal training in order to maximize the simulator's utility.

THIS PAGE INTENTIONALLY LEFT BLANK

III. STUDY METHODOLOGY AND MODELING EFFORT

This chapter introduces a proposed problem solution to answer the problems statement in Chapter I; namely, fielded expendable countermeasure systems cannot adequately protect friendly aircraft from modern radar-guided threats. The solution includes developing a low-fidelity simulation to allow designers and engineers the ability to examine the design space of a new system that can fill this capability gap. The chapter introduces the engagement scenario on which the simulation is based as well as identifies the engagement variables that require modeling. The chapter discusses the individual models of the simulation in detail including the mathematical equations used to represent the scenario elements. Individual models represent the radar system, missile system, aircraft, EAD, and environment. All equation variables, their definitions, and the units are contained in Appendix A.

A. PROPOSED PROBLEM SOLUTION

In order to facilitate the design of a new EAD system by the U.S. military, the first step is to develop a low-fidelity simulation that allows for low-cost exploration of the design space, fulfilling the request of Vice Admiral Grosklags. The basis for this thesis is the construction of a simulation that will receive input from a user on the characteristics of a radar-guided threat, aircraft, expendable, and environment. The models of the systems will be equation-based and physics-based approximations. The simulation executes hundreds of times to collect samples of the decoy's performance based on the variation of stochastic variables. Statistical analysis of the data then determines the decoy's effectiveness against the selected radar-guided threat.

B. MODELING AND SIMULATION BASED SYSTEMS ENGINEERING DISCUSSION

This study uses a modeling and simulation-based systems engineering (MSBSE) approach, employs scenario methodologies, and experimentation using a low-fidelity computer simulation to identify the required key performance parameters for a new radar decoy system. According to the INCOSE SE Vision 2020 point paper, "model-based

systems engineering (MBSE) is the formalized application of modeling to support system requirements, design, analysis, verification and validation activities beginning in the conceptual design phase and continuing throughout development and later life cycle phases" (INCOSE-TP-2004-004-02 2007).

The difference between a model and a simulation is "a model is a physical, mathematical, or logical abstract representation of a system entity, while a simulation is the implementation of a model over time that brings the corresponding model to life" (Gianni et al. 2015). MSBSE incorporates models in the context of a simulation to evaluate the properties of a complex system, in a specific environment, and typically allows for execution on a time scale, to provide a more comprehensive analysis of the design space than can be achieved with MBSE alone. This thesis employs models to represent the various individual elements of helicopter and missile engagement, which include the operational scenario, radar and weapon systems, aircraft, decoy systems, environment, and decision processes. Using these models within a simulation construct allows for the analysis and design of the SOI.

C. SIMULATION ENGAGEMENT SCENARIO

To employ an MSBSE approach requires development of an acceptable model. The computer simulation scenario uses an open-ocean engagement of a friendly helicopter by an enemy surface vessel. An open-ocean engagement removes the possibility of terrain masking from the friendly helicopter's repertoire of defensive tactics. This thesis supports an EAD system in development by NAVAIR, which will be used on naval aircraft in the maritime environment. Additionally, open-ocean reduces the possibility of multi-path effects playing a role and simplifies their calculation when they do occur.

The scenario employs the MH-60S helicopter because it is the most predominant U.S. Navy rotary-wing aircraft and fulfills the anti-surface warfare mission set. Additionally, the inherent speed and maneuverability limitations of the airframe preclude the possibility of out maneuvering or out running the threat missile. Lastly, this aircraft represents the worst-case scenario in terms of radar cross section (RCS) of naval aircraft because of complex interactions of the airframe and rotor systems. If an EAD is capable of

decoying a radar-guided threat when employed from a helicopter, then logically the effectiveness should improve when employed from a fighter or transport aircraft that has greater maneuverability and speed.

The frequency range of interest for this thesis is from 2 – 18 Ghz. To validate the simulation later in the study, the threat radar chosen was the Castor 2 J/C radar shown in Figure 8. It operates within the frequency range of interest and is a commonly used fire control radar on foreign naval vessels. The missile systems paired with the Castor 2 J/C are semi-active guided systems. According to a one-on-one interaction with Dr. Robert Harney (2017), bistatic radars best represent semi-active guided systems with the radar being the transmitter and the missile being the receiver. According to Streetly's *Jane's Radar and Electronic Warfare Systems 2005–2006*, the Castor 2 J/C radar is a broadband, J-band, monopulse-Doppler tracking radar. It has a peak power of 30 kilowatts, a maximum range of 30 km, and a tracking accuracy of 5 m. It also incorporates an EO/IR suite for passive tracking and target acquisition (Streetly 2006). Table 3.1 covers the Castor 2 J/C specifications that were derived from *Jane's Radar and Electronic Warfare Systems* and Air Power Australia, an independent defense think tank.

Table 1. Castor 2 J/C Specifications. Source: Streetly (2006); Air Power Australia (2014).

Peak Power	30,000+ watts
Frequency Operating Band	J-band; 15.7 – 17.7 GHz
Range	0.7 – 30 km
Tracking Accuracy	5 m
Pulse Repetition Frequency (PRF)	3600 – 7200 pps
Pulse Duration	7.4 – 7.6 μs
Transmitter Gain	43 dB
Beam width	0.67° elevation

Figure 8. Type 345 (Castor 2 J/C) Engagement Radar.
Source: Air Power Australia (2009).

Figure 9 represents the engagement scenario flow diagram. A friendly aircraft will approach a naval surface vessel. The naval surface vessel will be radiating its detection and tracking radars in an effort to detect the aircraft. Once the aircraft is in range of the targeting radar, the radar-guided threat engages the aircraft. The aircraft, having detected the engagement, will deploy an EAD in an attempt to defend against the threat. Either the decoy will succeed and the missile will fail to destroy the aircraft, or the missile will successfully impact the aircraft. Red boxes represent the inputs and outputs related to the radar and missile models. Blue boxes are the inputs and outputs of the aircraft model. Green boxes represent the inputs and outputs related to the EAD model. The inset image shows the Department of Defense Acquisition Framework Operational View (OV-1). This is a high-level representation of the engagement that the simulation replicates.

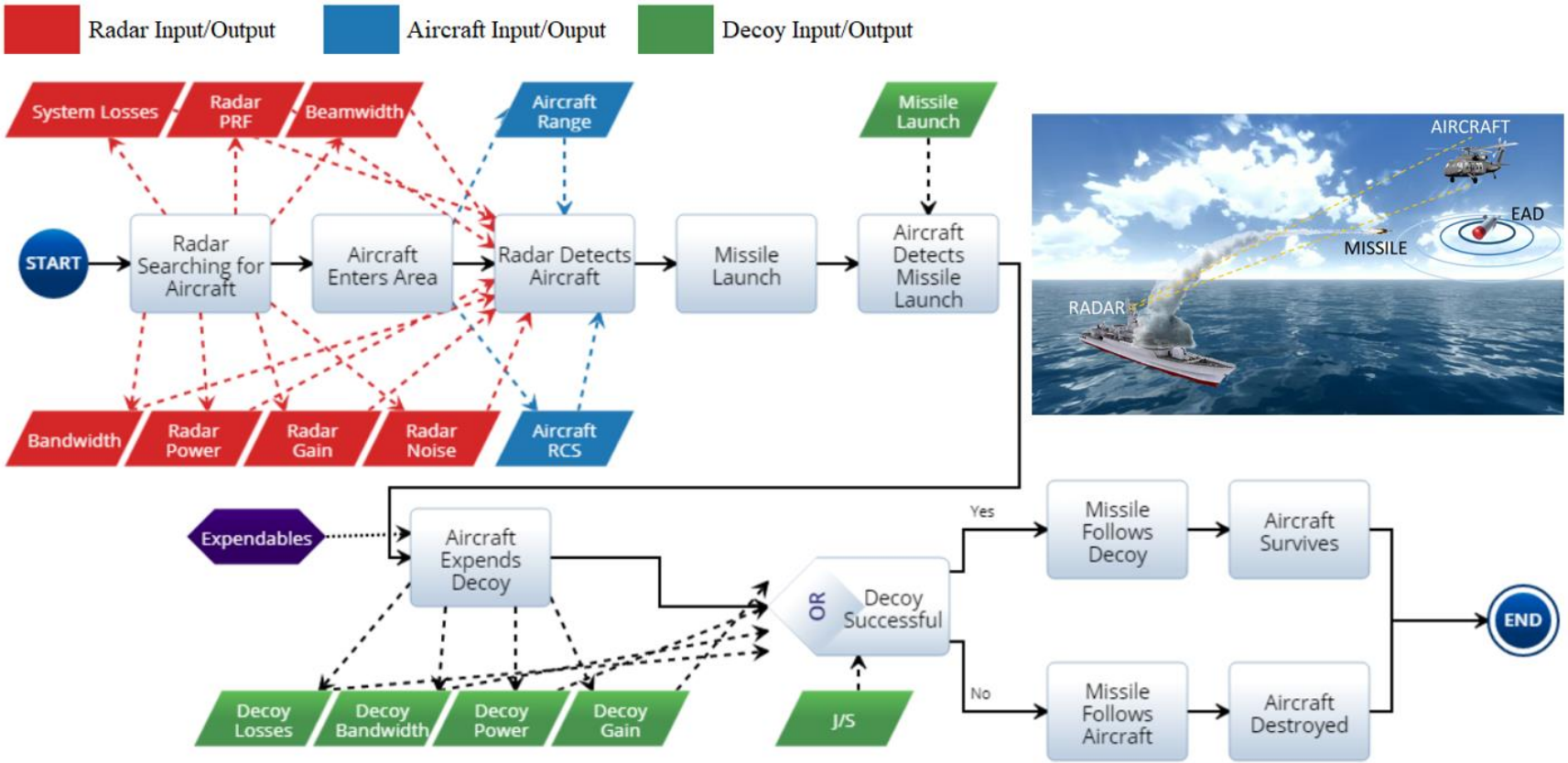

Figure 9. Engagement Scenario Flow Diagram and OV-1

D. RADAR AND WEAPONS SYSTEMS MODEL

The radar model uses the radar range equation to represent the radar and missile systems. This equation provides the carrier-to-noise ratio (CNR) of the radar. The CNR is the ratio of the radar-generated signal that returns from a target to the noise that the radar receives from background phenomena. The greater the CNR, the greater the probability of detection by the radar. This factor is important because it defines the ability of the radar to detect a target. The radar range equation, derived from Harney (2013a), is given as

$$CNR = \frac{P_T L_T L_R G_T A_R \sigma e^{-2\alpha R}}{16\pi^2 (kTBF) R^4} \tag{1}$$

Because the semi-active guided missile represents a bistatic radar system, the author modified Equation 1 to differentiate between the transmitter and receiver ranges; that is to say, as the missile moves closer to the aircraft, the receiver range will decrease while the transmitter range remains approximately the same. Equation 2 reflects these changes and applies to the missile system only.

$$CNR = \frac{P_T L_T L_R G_T A_R \sigma e^{-\alpha (R_T + R_R)}}{16\pi^2 (kTBF) R_T^{\,2} R_R^{\,2}} \tag{2}$$

Research provides some of the values for the variables such as power and gain. Other variables must use reasonable assumptions. Assumptions made for the model include:

- transmitter and receiver loss factor of -2 dB (Brooker 2007, 299)
- clear weather resulting in no atmospheric attenuation due to the frequency being less than 20 GHz (Harney 2013c, 96)
- electronic temperature is 290K (Brooker 2007, 283)
- Radar receiver on missile has a radius of 0.07 m. The HQ-7 missile is one of the missiles commonly paired with the Castor 2J/C and has a diameter of

0.15 m according to Air Power Australia; therefore, a receiver radius of 0.07 m is reasonable. (Air Power Australia 2014)

- Noise Factor is 4 dB (Brooker 2007, 298)
- The receiver area for both the missile and the radar is circular.

In order to improve detection probability, modern radar systems employ pulse integration to improve detection probability. They do this by collecting many return pulses and integrating them over time instead of using individual pulses, which can vary in intensity between subsequent pulses. Equation 3 from Brooker (2007) represents a rotating radar's hits per scan of the radar pulses on the target. This is useful for determining total pulses received so that the radar can integrate the pulses to improve detection probability. This equation is in the model for future use; however, the Castor 2 J/C does not rotate. For this reason, the author assumes 100 hits per scan for the purposes of the simulation. Derivation of the integration improvement factor comes from Figure 10 after determining the hits per scan. The user will use the hits per scan calculated in Equation 3 to enter the chart from the bottom at the appropriate value, find where the line intersects the desired Swerling case (discussed in Aircraft Model Section III.E), and read the associated integration improvement factor off the left side of Figure 10.

$$n_b = \frac{\theta_b f_p}{\dot{\theta}_s} \tag{3}$$

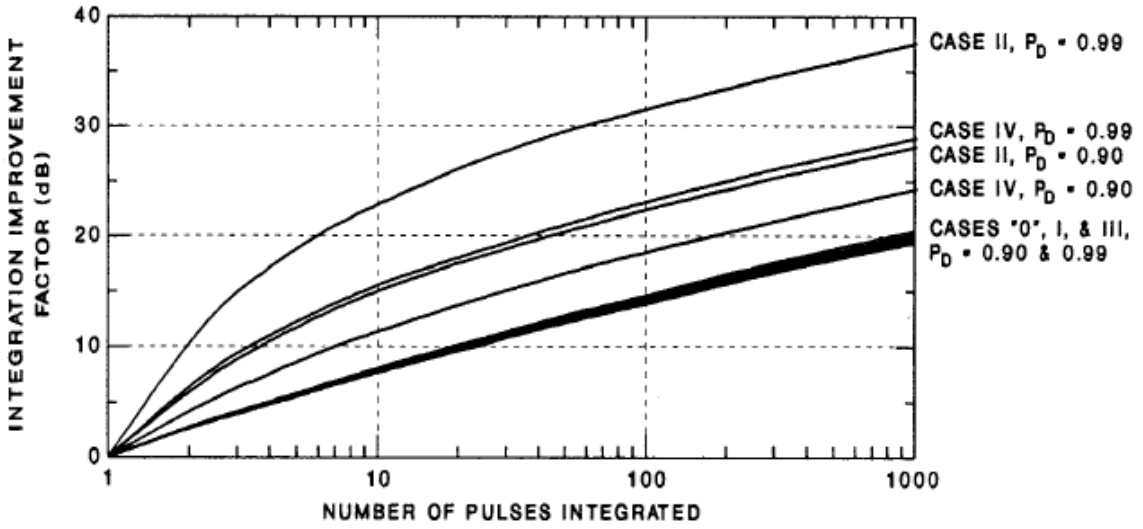

Figure 10. Integration Improvement Factor. Source: Harney (2013a, 370).

A radar operates with a central frequency of interest known as the modulating frequency; however, due to the method of generating the radar pulse by the transmitter, the receiver takes in some of the surrounding frequency bands as well. This is known as the radar bandwidth and it is the difference between the upper and lower cut-off frequencies that surround the modulating frequency. The wider the bandwidth, the more noise allowed into the system and the less sensitive the radar system becomes; however, a narrow bandwidth might also distort the radar pulse shape resulting in degradation of receiver performance (Payne 2010, 36–37). Equation 4, adapted from Brooker (2007), provides a method for calculating an unknown radar bandwidth when given the pulse width. Table 2 comes from Brooker (2007) and lists the efficiency of non-matched filters. In keeping with planning for the worst-case scenario, the author assumes that the radar will use a Gaussian matched filter with a Gaussian pulse signal that results in no loss of signal to noise ratio on the part of the receiver. This gives a Bτ value of 0.44.

$$\varepsilon = B\tau \tag{4}$$

Table 2. Efficiency of Non-matched Filters. Source: Brooker (2007, 290).

Input Signal Shape	Matched Filter Characteristic	Optimum $B.\tau$	Loss in SNR compared to Matched Filter (dB)
Rectangular Pulse	Rectangular	1.37	0.85
Rectangular Pulse	Gaussian	0.72	0.49
Gaussian Pulse	Rectangular	0.72	0.39
Gaussian Pulse	Gaussian	0.44	0 (matched)
Rectangular Pulse	Single tuned circuit	0.4	0.88
Rectangular Pulse	Two cascaded tuned circuits	0.613	0.56
Rectangular Pulse	Five cascaded tuned circuits	0.672	0.5

The probability of false alarm is the chance that radar noise will exceed the detection threshold, resulting in a false detection. False detections are undesirable because they utilize crew resources and cause distraction to the operator, which may result in missing an actual target. With Equation 5, adapted from Harney (2013a), one can calculate probability of false alarm (P_{fa}) when one knows the bandwidth and time between false alarms. Without knowing the time between false alarms for the Castor 2J/C, the author assumes that T_{fa} is two hours (7200 seconds). This assumption derives from the author's experience that target radars only operate for a short duration during an engagement and a low T_{fa} is acceptable.

$$P_{fa} = \frac{1}{T_{fa} B} \tag{5}$$

E. AIRCRAFT MODEL

The choice of aircraft brings with it the difficulties of calculating radar reflection characteristics brought on by the complex geometry and spinning rotor systems. The primary characteristic of these radar reflections is known as the radar cross section (RCS). The RCS in important because the greater the RCS, the greater the CNR of a radar return resulting in an increased probability of detection.

In order to determine the approximate RCS of an MH-60S, a MATLAB program called POFACETS, developed by Hellenic Air Force Major Filippos Chatzigeorgiadis at NPS in 2004, calculates the bistatic radar cross section. A basic 3D representation of the MH-60S was created using published and derived dimensions. A rectangle box represents the fuselage, a wedge the tail boom, flat plates for the wings, rotors, vertical, and horizontal stabilizers, ellipses for the cockpit and nose, a sphere for the multi-spectral targeting system (MTS), cylinders for landing gear, and cylinders with ogive nose cones for the Hellfire missiles. Figure 11 is a display of the basic 3D model. All axes are in meters.

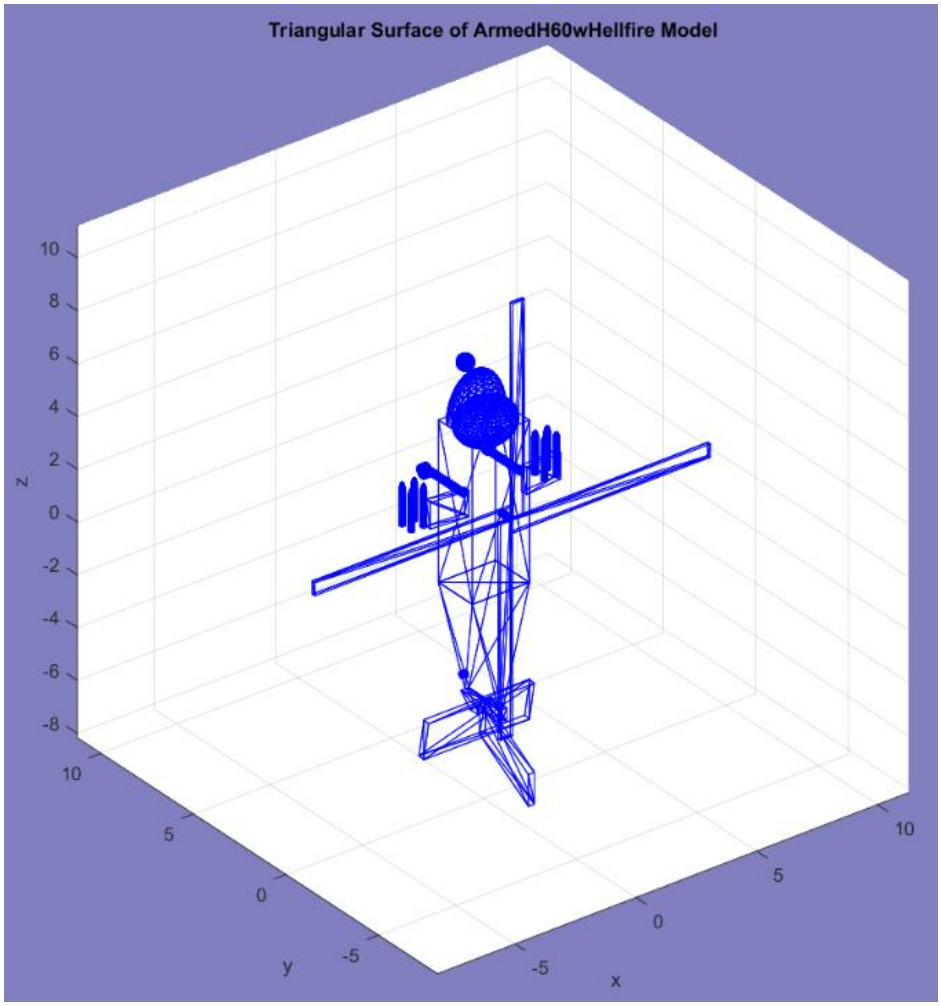

Figure 11. Basic 3D Model of MH-60S with Hellfire. Source: POFACETS MATLAB 2016a.

The POFACETS program allows the determination of radar cross section from any model angle in decibels per square meter. The author used POFACETS to calculate the bistatic radar cross section for the model in 1 GHz increments from 2 to 18 GHz. Since the Castor 2 J/C operates between 15.7 and 17.7 GHz, the author chose 16 GHz for the model. Figure 12 shows the polar plot of the RCS at 16 GHz and 0° elevation from 0 to 360 degrees. The vertical axis is the RCS in decibels per square meter. Based on operational experience and the results of the POFACETS calculation, the author assumes an average RCS of 24 dBsm. This value falls within the bounds of realistically expected values when compared to values provided in Harney's text (2013b, 108).

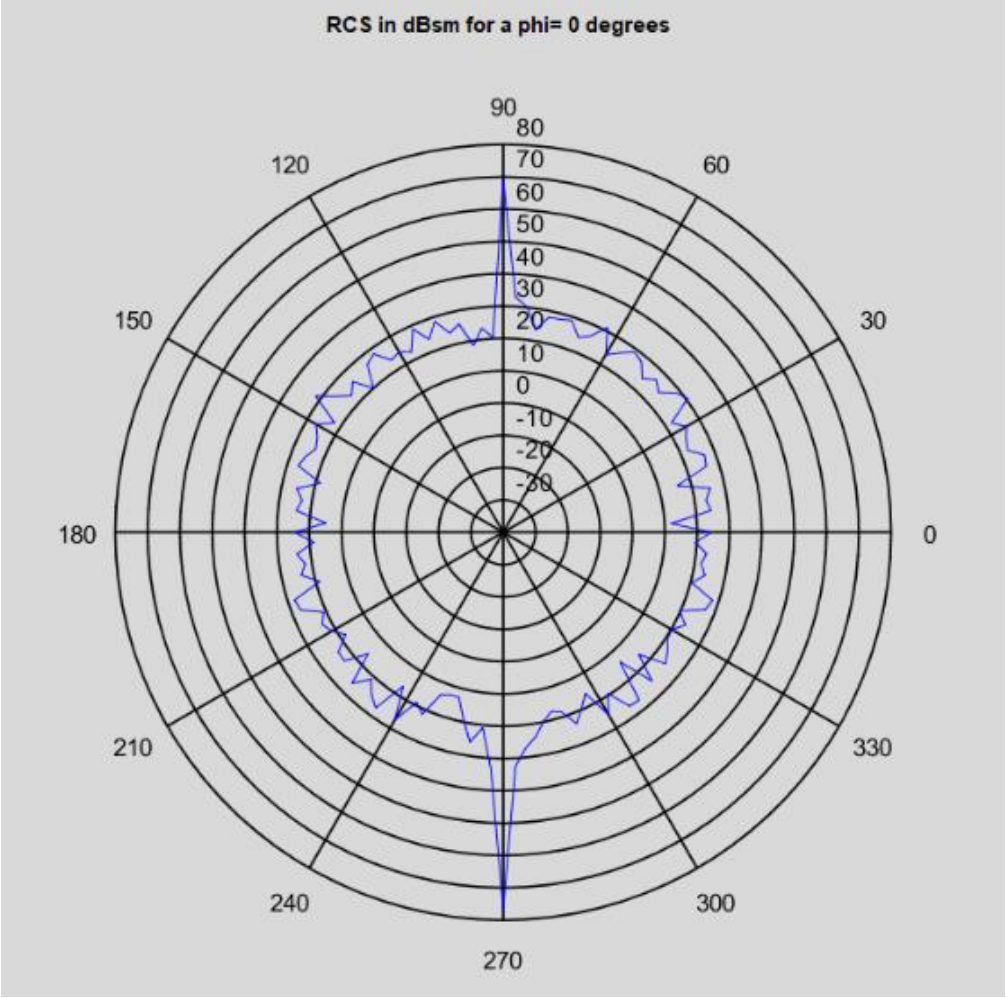

Figure 12. MH-60S Bistatic Radar Cross Section at 16 GHz, 0° Angle of Elevation. Source: POFACETS MATLAB 2016a.

Most real-world objects do not exhibit a steady state RCS. Interactions between reflections off complex vehicle geometries and spinning parts will cause the RCS to fluctuate in intensity. Because of the reflective geometry and rotor system of the MH-60S, it exhibits fluctuations in its RCS. Swerling models characterize these fluctuations. Figure 13 shows the additional CNR required in order to detect a fluctuating target over a non-fluctuating one. The worst-case scenario is a target exhibiting Swerling Cases I and II characteristics. Any realistic probability of detection (≥0.90) requires a greater CNR for Swerling I/II than it does for Swerling III/IV. Therefore, Swerling Case II best represents the worst case scenario for fluctuating characteristics of the helicopter model; though Swerling Case IV likely better represents a helicopter due to the fast fluctuations of a main and tail rotor.

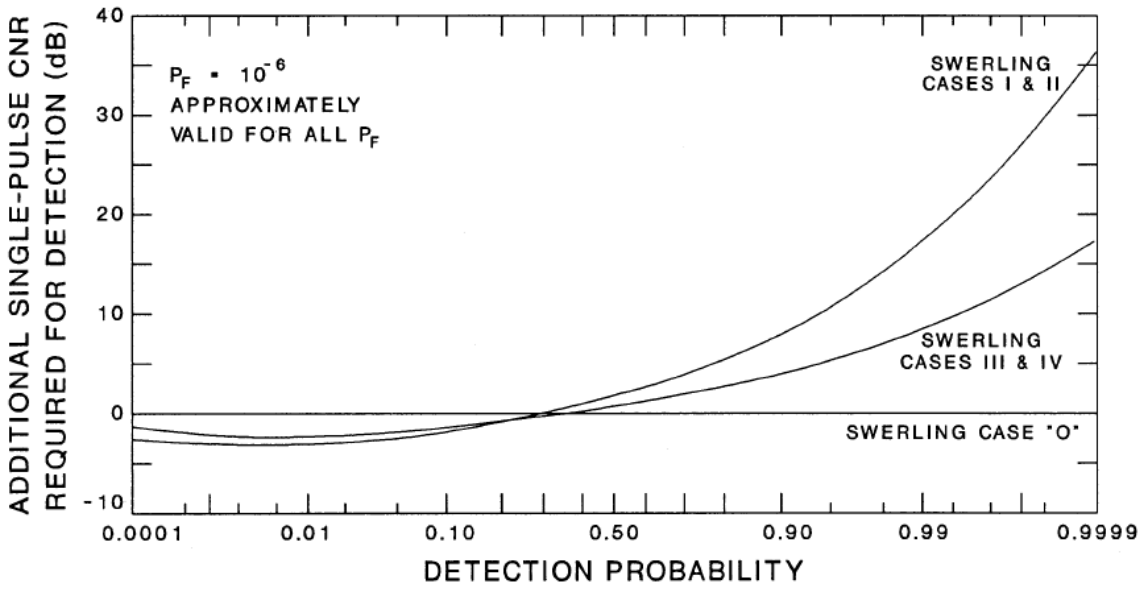

Figure 13. Additional Carrier-to-Noise Required for Fluctuating Targets. Source: Harney (2013a).

The simulation allows the user to choose a desired probability of detection. For the purposes of this thesis, the author chooses a probability of detection of 0.90. Combining the desired probability of detection with the probability of false alarm calculated by Equation 5, helps determine the CNR required by the radar to detect a Swerling Case II

target. This Swerling CNR is compared to the CNR produced by the target return from Equation 2 to determine whether detection occurs. Equation 6 from Harney (2013a) is the closed form solution for Swerling Case II only. Alternatively, one may use receiver operation characteristic (ROC) curves, shown in Figure 14, to analytically determine the CNR required.

$$P_D = P_F^{(1/(1+CNR))} \tag{6}$$

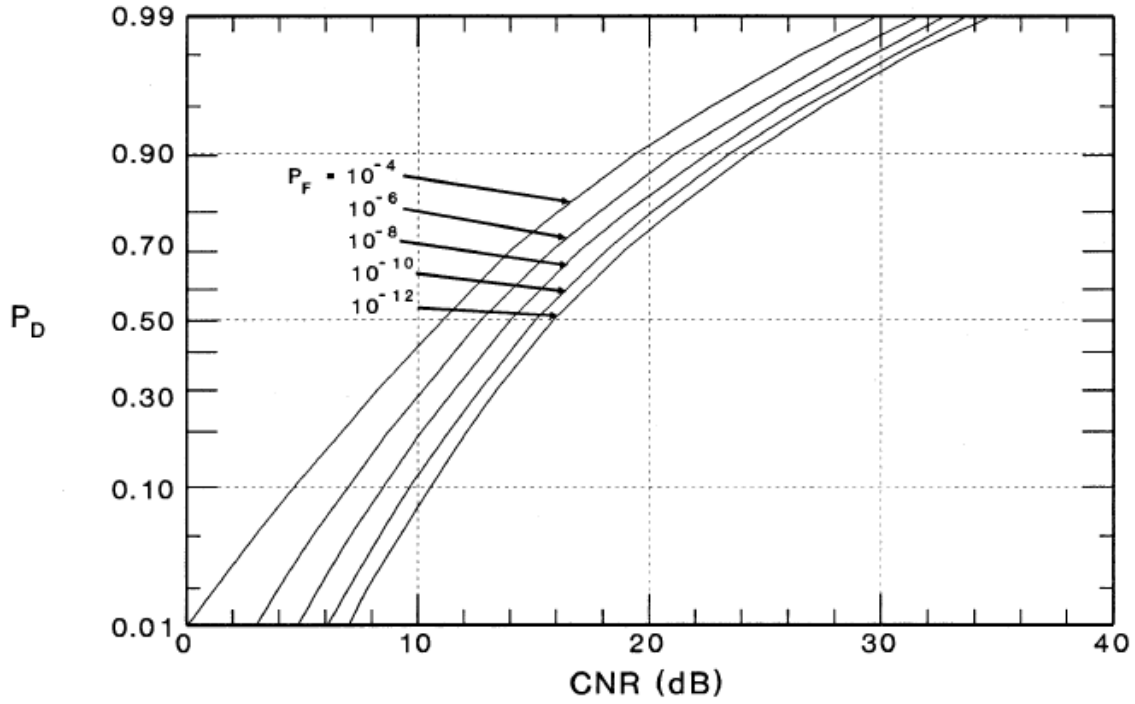

Figure 14. Receiver Operating Characteristic Curves for Swerling II Statistics. Source: Harney (2013a).

a. Flight Path

The kinematic equations of motion are mathematical representations that explain the movement of objects over time. With a known starting range, velocity, and acceleration, one can calculate the position of an object after a known duration of time. The equations are separated into the vertical and horizontal components. For the purposes of the model,

the author assumes the flight path of the aircraft to be a straight, level, and un-accelerated. Therefore, the aircraft model only uses the horizontal component. This movement model is used to calculate the change in range of the aircraft as the simulation progresses as well as provides a portion of the EAD's forward velocity on deployment. The horizontal component kinematic equation in Equation 7 represents the flight path where acceleration is zero.

$$R = R_0 + V_x t + \frac{1}{2}\cancel{a_x t^2} = R_0 + V_x t \tag{7}$$

F. EAD MODEL

The jam-to-signal ratio (J/S) of a decoy is the ratio of the signal power produced by the decoy to the signal power produced by the target radar return. A J/S of greater than one is desirable for a decoy. If the J/S is greater than one, the decoy is able to produce a signal that is greater than the return signal coming from the target resulting in reduced detection probability. This is a critical measure for the simulation and defines one of the primary measures of performance of the system. The simulation uses this equation to determine whether or not the EAD is successful.

Decoys that record and repeat a radar signal are known as deception jammers. A deception jammer best represents an EAD. Equation 8, adapted from Harney (2013c), best represents these types of jammers. Since, per the scenario, the radar is engaging the friendly helicopter, the author assumes that the radar is pointing directly at the aircraft and SLL is 1 (0 dB). Equation 3.8 applies to the jam to signal ratio for the radar only.

$$\frac{J}{S} \approx \frac{P_J L_T G_J \left(SLL\right) 4\pi {R_T}^4}{P_T L_R G_T \sigma {R_J}^2} \tag{8}$$

Because the radar is being treated as a bistatic system, as the missile moves closer to the target the range from the receiver decreases while the jammer range and radar range remain approximately the same ($R_T \approx R_J$). Therefore, Equation 8 becomes Equation 9 when representing the missile.

$$\frac{J}{S} \approx \frac{P_J L_T G_J \left(SLL\right) 4\pi {R_T}^2 {R_R}^2}{P_T L_R G_T \sigma {R_J}^2} \approx \frac{P_J L_T G_J \left(SLL\right) 4\pi {R_R}^2}{P_T L_R G_T \sigma} \tag{9}$$

The aircraft only had horizontal flight path components; however, the EAD has both horizontal and vertical components that require modeling. The kinematic equations of motion in Equations 10 and 11 represent the flight path and velocities of the EAD in the horizontal and vertical directions. In the model, the user can change the acceleration and initial velocity of the EAD to simulate the type of deployment such as falling under parachute or free fall. These equations will determine the change in range and altitude of the EAD during the engagement scenario as well as the change in velocity. The author assumes that acceleration is constant.

$$\begin{aligned} R &= R_0 + V_x t + \frac{1}{2} a_x t^2 \\ H &= H_0 + V_y t + \frac{1}{2} a_y t^2 \end{aligned} \tag{10}$$

$$\begin{aligned} V_x &= V_x + a_x t \\ V_y &= V_y + a_y t \end{aligned} \tag{11}$$

G. ENVIRONMENT MODEL

Multipath is a phenomenon that occurs when the radar signal bounces off the ground plane before it bounces off the target. This creates multiple paths for the radar signal to return to the radar receiver. Typically, four paths exist and Figure 15 shows the geometry. These paths include a direct path from the radar, to the target, and back to the receiver (A→C→A). Another path involves the signal bouncing off the ground plane, hitting the target, and returning to the radar the way it came (A→B→C→B→A). The last two paths involve either a direct path to the target and return by bouncing off the ground plane (A→C→B→A) or vice versa (A→B→C→A). Multipath allows aircraft to hide in null zones where the destructive interference caused by multiple radar returns results in loss of radar detection capability. The multipath model is only valid when the angle between the ground bounce point and the target (alpha + beta) is less than the beam width

elevation. Equation 12, from Harney (2013a), determines the validity of this criterion. If multipath criteria are met then the effects can be calculated utilizing Equation 13, adapted from Harney (2013a). If the ratio is less than one, then the target is in a null zone and is not detectable. For the purposes of this thesis, multipath is not considered in the determination of EAD success or failure; however, it is included for future development of the simulation to add greater fidelity.

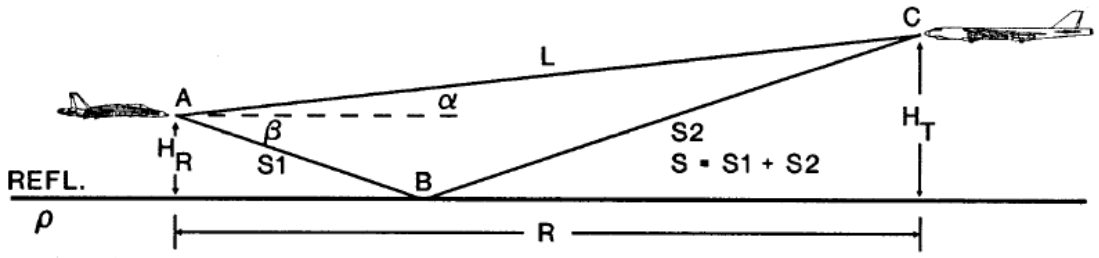

Figure 15. Geometry Definition of Multipath Returns. Source: Harney (2013a)

$$\alpha + \beta = \tan^{-1}\left(\frac{H_T - H_R}{R}\right) + \tan^{-1}\left(\frac{H_T + H_R}{R}\right) \leq \theta_{BW} \tag{12}$$

$$\frac{P_R}{P_0} \approx 16\left(\frac{R_{DET}}{R}\right)^4 \sin^4\left(\frac{\left(\frac{2\pi}{\lambda}\right)H_T H_R}{R}\right) \tag{13}$$

Sea surface backscatter is a phenomenon that occurs when the radar beam is sufficiently wide that some radar energy is reflected off the surface of the ocean. This return, if of sufficient magnitude, can mask a target signal. The magnitude of this return known as sea surface clutter RCS is dependent on sea state, beam width, and the range resolution of the radar. In the simulation's current state, the sea surface clutter RCS is overwhelmed by the target RCS. Therefore, the computations are not used for the overall measure of performance of the EAD, but they are in place for further development. Equation 14, adapted from Harney (2013b), calculates the sea surface clutter RCS.

$$\sigma_{SC} = R\theta_{BW}\Delta R\sigma_0 \tag{14}$$

The radar range resolution is the length of the imaginary box created in space by the pulse duration. Equation 15 from Harney (2013b) calculates the range resolution.

$$\Delta R = \frac{\tau c}{2} \tag{15}$$

Table 3 is an example of a look-up table containing empirically derived data showing the mean backscatter coefficient of various wavelengths depending on grazing angle, sea state, and radar wave polarization. The grazing angle of the incident radar wave can be calculated using Equation 16. This thesis defines grazing angle (θ_{GA}) as the angle of elevation of the center of the radar beam to the target minus half the elevation beam width.

$$\theta_{GA} = \tan^{-1}\left(\frac{H_T - H_R}{R}\right) - \frac{\theta_{BW}}{2} \tag{16}$$

Table 3. Normalized Mean Backscatter Coefficient for 0.3° Grazing Angle. Source: Harney (2013b, 115)

SEA STATE	POL.	REFLECTION COEFFICIENT in dBsm/m^2						
		0.5 GHz	1.25 GHz	3.0 GHz	5.6 GHz	9.3 GHz	17 GHz	35 GHz
0	V	—	-83	—	—	—	-63	-55
	H	—	—	-83	-79	-74	—	—
1	V	—	-78	-64	-60	-58	-54	-46
	H	—	—	-74	-68	-66	-58	—
2	V	-80	-73	-62	-55	-52	-52	-43
	H	-78	—	-66	-60	-56	-53	—
3	V	-78	-70	-58	-50	-45	-47	-40
	H	—	-68	-60	-50	-46	-42	—
4	V	-75	-65	-57	—	-43	-44	-38
	H	—	—	-55	—	-42	-39	—
5	V	-73	-64	-52	—	-39	-39	-35
	H	—	-64	-52	-44	-39	-38	—
6	V	—	—	—	—	-34	-37	-31
	H	—	—	-46	—	-34	-37	—

After choosing the appropriate mean backscatter coefficient, the value is substituted into Equation 17, adapted from Harney (2013b), in order to calculate the sea clutter CNR.

$$CNR_{SC} = \frac{P_T L_T L_R G_T A_R (R\theta_{BW} \Delta R \sigma_0) e^{-2\alpha R}}{16\pi^2 (kTBF) R^4} \tag{17}$$

H. PROBABILITY DENSITY FUNCTIONS

One can plot the probability density functions of the noise and signal plus noise to provide a visual comparison of the target radar return intensity to background noise. The noise inherent in the radar is often narrow-band filtered and results in a Gaussian probability distribution. Equation 18, from Harney (2013a), represents the Gaussian noise. V is the voltage of the noise return and V_0 is the root mean squared noise level.

$$p_N(V) = \left(\frac{V}{V_0}\right)^2 e^{-\frac{V^2}{2V_0^2}} \tag{18}$$

The probability density function for Gaussian noise is altered when a target is present. The radar return adds to the Gaussian noise and the probability density function becomes Rician. Equation 3.19, from Harney (2013a), is the probability density function for a non-fluctuating return signal plus noise.

$$p_{S+N}(V) = \left(\frac{V}{V_0}\right)^2 e^{-\frac{\left(V^2+A^2\right)}{2V_0^2}} I_0\left(\frac{VA}{V_0^2}\right) \tag{19}$$

I_0 is a Bessel function of imaginary argument and is a function of (VA/V_0^2). A is the voltage of the target return. If the CNR of the target return is known, Equation 20 from Harney (2013a) can substitute CNR for A. After determining the voltage of the target return, it can be substituted into Equation 20 and the probability density function can be graphed.

$$CNR = \frac{A^2}{V_0^{\,2}} \tag{20}$$

I. VERIFICATION AND VALIDATION OF THE INTEGRATED SIMULATION MODEL

The Cartwright Expendable Active Decoy Simulator (CEADS) is the result of the integration of all of the previous models into a single simulator. Each of the aforementioned models is integrated into the Excel-based simulation on individual tabs. A specific tab represents each of the following elements of the CEADS: EAD, radar, missile, multipath, and sea surface clutter. The models are cross-linked so that if a shared value changes on one tab, it changes on all corresponding models that use the same value. Appendix B contains examples of each model and Appendix C is the simulator.

CEADS accepts input from the user on the radar, missile, aircraft, EAD, and environment variables. The performance parameters of the missile, aircraft, EAD, environment, and Castor 2 J/C radar from Table 3.1 are input into the associated models. The radar, missile, and EAD models calculate the CNR of the aircraft as seen by the radar or missile and compare them to the required CNR for a specified detection probability. The EAD model goes further by also calculating the CNR generated by the EAD given the EAD performance parameters input by the user. The result is either non-detection of the aircraft due to the CNR being below the detection threshold, aircraft detection because the CNR is above the threshold, or aircraft non-detection because the EAD CNR causes a jam-to-signal ratio of greater than one. It also provides a visual simulation of the engagement showing the decoy effectiveness. Figure 16 is an example of the visual simulation.

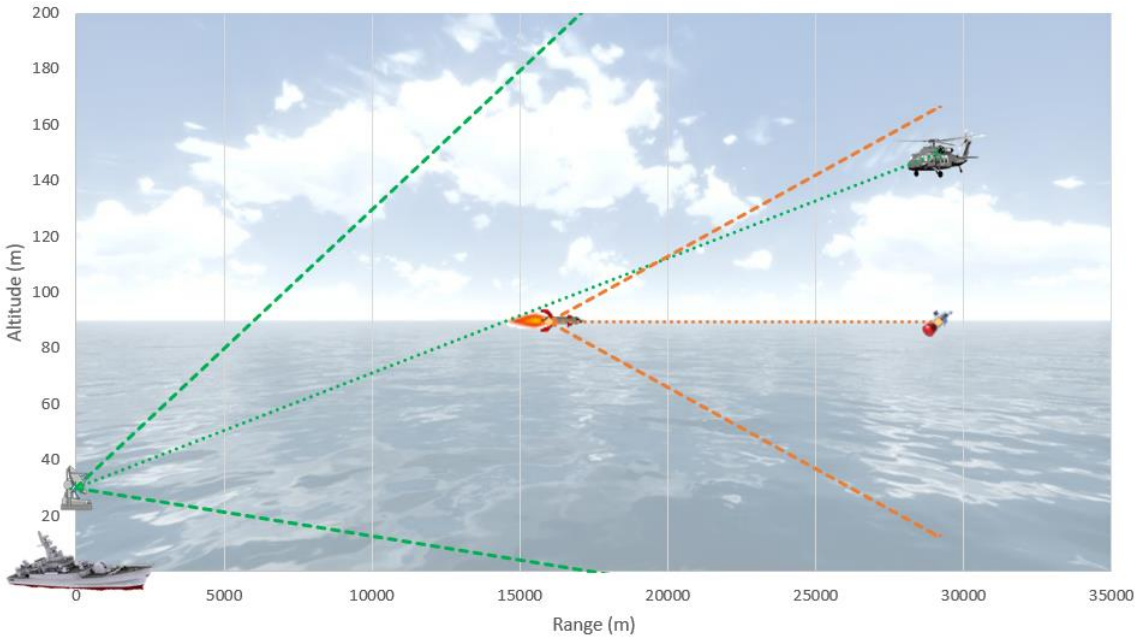

Green lines represent the radar. Orange lines represent the missile. Dashed lines are the upper and lower beam width edges and dotted lines are the beam center.

Figure 16. Visual Simulation of Engagement

In order to verify that the simulator is operating as intended, the author analyzed the results of a simulator run and compared them to hand calculations. Figure 18 in chapter IV shows an instantaneous calculation of missile CNR. The author used Equation 2 to calculate the missile CNR and compared it to the CNR calculated by the simulator. The result of the hand calculation shows the same missile CNR achieved by the simulator at the bottom of Figure 18. Similar computations and comparisons for all equations in the model verify that the equations constructed from a variety of experts in the corresponding fields are correctly implemented in the simulator and produce appropriate values.

$$\mathrm{CNR} = \frac{P_T L_T L_R G_T A_R \sigma e^{-\alpha(R_T+R_R)}}{16\pi^2 (kTBF) {R_T}^2 {R_R}^2}$$

$$\mathrm{CNR} = \frac{(30424)(.52)(.6)(19808.69)(.0154)(3.01)}{16\pi^2 (1.38\times10^{-23})(290)(2.2\times10^{5})(6.85)(24367.5)^2 (24367.5\text{-}11500)^2} = 93.0$$

Based on the author's experience, the outputs provided by the simulator are reasonable and acceptable. The simulator uses the values to calculate the jam-to-signal ratio, which it then uses to determine the instantaneous success or failure of the EAD. The

simulator demonstrates that increasing EAD power or gain results in a subsequent instantaneous increase in jam-to-signal ratio, which is to be expected. It then follows that a greater jam-to-signal ratio results in a greater likelihood of EAD success. As the author will demonstrate in chapter IV, the data obtained through experimentation supports this statement. The validation of CEADS proves it to be a useful modeling and simulation based systems engineering tool that can reduce design and testing time of future EAD systems.

J. MEASURES OF EFFECTIVENESS

The simulation allows a systems engineer to examine the key measure of effectiveness (MOE) for the EAD system. These key MOEs drive the value of a new system to the stakeholder and drive the requirements that the systems engineer will set for the system. The key MOE for this simulator focuses on whether or not the EAD can successfully drive the missile to a geometry that it is no longer able to engage the aircraft. This happens when the J/S produced by the EAD is significant enough that the missile remains focused on the EAD as it falls away from the aircraft until the missile's range and altitude no longer permit it to receive the radar returns off the target. At this point, the MOE declares the simulator run a success and moves on to the next run. If the EAD fails to lure the incoming missile, then the missile's focus will remain on the target aircraft and will eventually strike the target resulting in a failure.

K. FACTORS

The factors that the author believes will have the greatest outcome on the success of the EAD are those factors that are inherent to the system. These factors are the variables contained in Equations 8 and 9 for jam-to-signal ratio. Those factors are EAD transmitter power, EAD loss factor, EAD gain, EAD bandwidth, and EAD deployment range. Other factors that the author believes to be significant, but are not necessarily captured in any equations, are EAD vertical and horizontal accelerations, and EAD vertical and horizontal velocities. These factors will have an effect on how long the EAD remains airborne and how quickly it can drive the missile to an unfavorable geometry. These 10 factors shown in Table 4 combine to create the design of experiments (DOE) for CEADS.

Table 4. Experimentation Factors

Factor	Description	Reason for Inclusion
EAD Transmitter Power	Power in watts produced at the EAD transmitter	Affects J/S
EAD Loss Factor	Percentage of remaining power prior to transmission	Affects J/S
EAD Gain	EAD energy focused in a specific direction	Affects J/S
EAD Bandwidth	Difference between upper and lower cutoff frequencies	Affects J/S
Vertical Acceleration	Vertical acceleration on deployment	Affects altitude which affects time of engagement
Horizontal Acceleration	Horizontal deceleration on deployment	Affects Range which affects J/S
Vertical Velocity	Vertical velocity on deployment	Affects altitude which affects time of engagement
Horizontal Velocity	Horizontal velocity on deployment	Affects Range which affects J/S
Deployment Altitude	Altitude of the aircraft at deployment	Affects time of engagement
Deployment Range	Range of the EAD from the missile at deployment	Affects J/S

L. EXPERIMENTATION

This thesis applies computer simulation and experimentation to examine the design space of the EAD system. Experimentation is a key component of knowledge acquisition. It is often infeasible or impractical to conduct physical experimentation with a system due to safety, money, time, or other constraints. In such situations, one may substitute computer model and simulation to represent the physical system and to understand the complex interactions between systems and the environment. Often these computer simulations may be preferred over physical experimentation and may reduce the risks to safety, cost, and schedule overruns. Computer experimentation allows analysts to assign causality, visualize interactions and trends, and develop mathematical expressions that relate factors with outcomes (Koehler and Owen 1996).

Sequential experimentation enables the researcher to focus on the most relevant areas of the design space. As such, a screening experiment first identifies the most relevant factors that affect the MOE, as well as significant interactions among the factors. The next set of experiments incorporates a nearly orthogonal Latin hypercube (NOLH) design. A NOLH allows for efficient exploration of the system design space and provides a good amount of information about the experimental region. NOLH also allows for simplified analysis of results though regression analysis and similar methods. This study examines 10 factors that the researcher believes have, or is uncertain about, the influence on the MOE. The DOE used for this thesis is an 11 x 33 NOLH from Cioppa (2002). Each design point is unique in its combination of values, and constitutes a singular instantiation of a potential EAD design. Figure 17 shows an example of the NOLH used in CEADS.

Units	Watts	dB	dB	10 kHZ	m/s^2	m/s^2	m/s	m/s	m	m
low level	1	0	1	1	0	0	0	0	15	1000
high level	10	10	10	1000	-9.8	10	-10	-10	300	25000
decimals	0	1	0	0	1	1	0	0	0	0
factor name	Jammer Transmitter Power (P_J)	Jammer Transmitter Loss Factor (L_T)	Jammer Gain (G_J)	Jammer Bandwidth (B_J)	EAD Initial ↑ Accel	EAD Initial → Accel	EAD Initial ↑ Velocity	EAD Initial → Velocity	EAD Initial Deployment Altitude	EAD Deployment Range
DP1	10	0.9	5	188	-8.6	6.3	-7	-5	300	17500
DP2	9	10	2	376	-4.6	1.9	-8	-3	273	11500
DP3	9	4.4	9	157	-0.3	5.9	-7	0	104	24250
DP4	6	8.8	10	407	-9.2	1.6	-8	-1	140	3250
DP5	9	0.3	5	220	-6.7	7.2	-4	-6	33	4000
DP6	10	9.4	4	282	-4.3	2.2	-2	-9	24	13750
DP7	7	4.7	10	251	0	6.6	-4	-9	264	1000
DP8	6	6.9	9	344	-8.9	2.5	-2	-10	166	23500
DP9	7	2.5	3	532	-7	3.1	0	-2	184	15250
DP10	8	6.6	4	688	-2.1	5.3	-1	-4	255	5500
DP11	7	2.2	8	969	-3.4	0.6	-1	-2	122	16000
DP12	8	7.2	7	938	-7.4	9.7	-5	-4	77	4750
DP13	6	1.6	3	563	-5.8	1.3	-10	-8	113	7750
DP14	9	5.9	4	875	-1.5	5.6	-9	-7	86	19750
DP15	7	1.9	9	906	-3.7	0	-7	-8	220	9250
DP16	8	6.3	6	1000	-8	9.1	-6	-7	247	19000
DP17	6	5	6	501	-4.9	5	-5	-5	158	13000
DP18	1	9.1	6	813	-1.2	3.8	-3	-5	15	8500
DP19	2	0	9	625	-5.2	8.1	-3	-7	42	14500
DP20	2	5.6	2	844	-9.5	4.1	-3	-10	211	1750
DP21	5	1.3	1	594	-0.6	8.4	-2	-9	175	22750
DP22	2	9.7	6	781	-3.1	2.8	-6	-4	282	22000
DP23	1	0.6	7	719	-5.5	7.8	-8	-1	291	12250
DP24	4	5.3	1	750	-9.8	3.4	-6	-1	51	25000
DP25	5	3.1	2	657	-0.9	7.5	-8	0	149	2500
DP26	4	7.5	8	469	-2.8	6.9	-10	-8	131	10750
DP27	3	3.4	7	313	-7.7	4.7	-9	-6	60	20500
DP28	4	7.8	3	32	-6.4	9.4	-9	-8	193	10000
DP29	3	2.8	4	63	-2.5	0.3	-5	-6	238	21250
DP30	5	8.4	8	438	-4	8.8	0	-2	202	18250
DP31	2	4.1	7	126	-8.3	4.4	-1	-3	229	6250
DP32	4	8.1	2	95	-6.1	10	-3	-3	95	16750
DP33	3	3.8	5	1	-1.8	0.9	-4	-3	68	7000

Figure 17. Nearly Orthogonal Latin Hypercube Experimental Design

M. DATA ANALYSIS

The author will conduct a sensitivity analysis by running multiple designs of experiments to determine the effects of changing variable ranges has on the probability of success. The author will then perform regression analysis to isolate significant main factors and two-way interactions. This regression analysis will determine whether any factors can be removed from the design of experiments. Finally, the author analyzes the results of the sensitivity analysis to determine which combination of factor values produce the highest probability of success, thereby highlighting the desired characteristics of the EAD and providing the design teams a focus in their efforts.

IV. SIMULATOR OPERATION

This chapter discusses the operation of the simulator. For CEADS to act as a true simulator that produces unique results each time it runs, a certain amount of randomness, or stochasticity, must be included. Equations 1 and 2 are deterministic, using the time-averaged values of the variables. However, the CEADS inserts stochastic values into the equations. The result is a discrete event simulation that incorporates randomness in its calculations. Specifically, the author chose to implement stochastic characteristics into the radar transmitter power, radar transmitter losses, missile receiver losses, missile noise factor, and the aircraft RCS. These variables, while not all inclusive of the possible stochastic values, represent the variables that the author believes have the greatest effect on detectability. Follow-on studies to this thesis may examine new variables.

In order to initialize CEADS for a simulation, the user inserts known values into the respective models. The user can enter nearly all required values into the EAD model. The EAD model is linked to the radar and missile models so that any shared values automatically update. For the purposes of this thesis, the author inserted the values from Table 1 into the radar section of the EAD model. Values not included in Table 1 are the assumptions stated in the radar and weapon systems model section III.D. Any cells highlighted in yellow require the user to input a value rather than choose from a slider bar. Figure 18 shows an example of the EAD model interface and inputs for each variable.

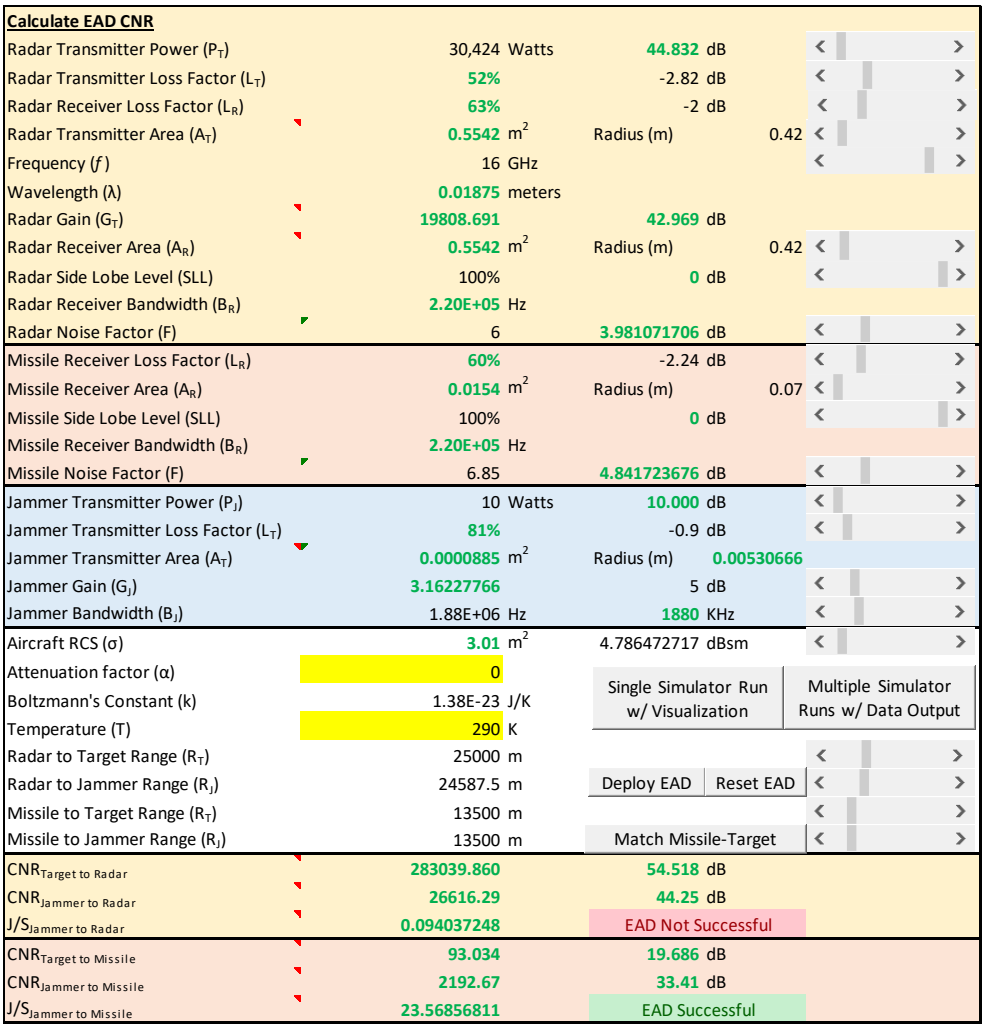

Figure 18. Inputs to the EAD Model

On the tab for the multipath model, the only inputs required are the radar altitude and the maximum detection range of the radar. Currently multipath effects do not influence the success or failure of the EAD; however, it is being included for future development of the simulator. On the tab for the surface clutter model, the only input necessary is choosing the sea state and polarization of the radar wave. Similarly, this model is not used to determine success or failure of the EAD, but is included for future development. Figure 19 shows the required inputs circled in red for the multipath and surface clutter models.

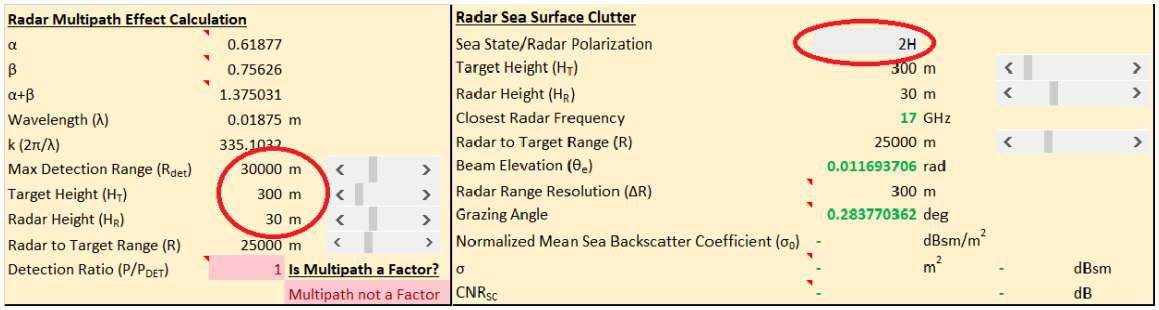

Radar Multipath Effect Calculation				Radar Sea Surface Clutter				
α	0.61877			Sea State/Radar Polarization	2H			
β	0.75626			Target Height (H_T)	300	m		
α+β	1.375031			Radar Height (H_R)	30	m		
Wavelength (λ)	0.01875	m		Closest Radar Frequency	17	GHz		
k (2π/λ)	335.1032			Radar to Target Range (R)	25000	m		
Max Detection Range (R_{det})	30000	m		Beam Elevation (θ_e)	0.011693706	rad		
Target Height (H_T)	300	m		Radar Range Resolution (ΔR)	300	m		
Radar Height (H_R)	30	m		Grazing Angle	0.283770362	deg		
Radar to Target Range (R)	25000	m		Normalized Mean Sea Backscatter Coefficient (σ_0)	-	$dBsm/m^2$		
Detection Ratio (P/P_{DET})	1	Is Multipath a Factor?		σ	-	m^2	-	dBsm
		Multipath not a Factor		CNR_{SC}	-		-	dB

Figure 19. Multipath and Sea Surface Clutter Models

The final inputs required are on the DOE tab. The user decides the minimum and maximum values of each variable. The NOLH determines the appropriate combination of variables in order to develop a design of experiments. Figure 20 shows an example of the variables and their low and high levels.

Units	Watts	dB	dB	10 kHZ	m/s^2	m/s^2	m/s	m/s	m	m
low level	1	0	1	1	0	0	0	0	15	1000
high level	10	10	10	1000	-9.8	10	-10	-10	300	25000
decimals	0	1	0	0	1	1	0	0	0	0
factor name	Jammer Transmitter Power (P_J)	Jammer Transmitter Loss Factor (L_T)	Jammer Gain (G_J)	Jammer Bandwidth (B_J)	EAD Initial ↑ Accel	EAD Initial → Accel	EAD Initial ↑ Velocity	EAD Initial → Velocity	EAD Initial Deployment Altitude	EAD Deployment Range

Figure 20. Design of Experiment Variable Levels

Once all input values are entered, the user returns to the EAD tab. The user makes the choice of a single or multiple runs by clicking one of the buttons shown in the white section of Figure 18. If the user chooses a single run by clicking "Single Simulator Run w/ Visualization," CEADS displays a visualization of the engagement in real-time as shown in Figure 16. If the user chooses to conduct multiple runs by clicking "Multiple Simulator Runs w/ Data Output," the simulator prompts the user for the design points to run, the number of runs for each design point, the radar transmitter power, and aircraft average RCS. When all runs are complete, CEADS saves the results from each run on individual tabs allowing for statistical analysis. Figure 21 shows an example of the raw data output. CEADS records simple statistical analysis to include proportion of runs resulting in success (mean), standard deviation, and 95% confidence intervals on the "DOE" tab for each design point shown in Figure 22.

Run #1						
Deployment Altitude (m)	300	Deployment Range (m)	17500			
Range to Target (m)	Radar Power (watts)	J/S	Aircraft RCS (dB)	Upper BW (m)	Out of Beamwidth	Hit?
25000	29406.71676	0	67.01287972	446.1729905	0	
24472.5	30235.57639	0	25.81166814	443.0887404	0	
23945	30356.52542	0	43.97835731	440.0044903	0	
23417.5	30742.7237	0	69.61543361	436.9202402	0	
22890	29546.40812	0	13.72556823	433.8359901	0	
22362.5	29717.05693	0	23.52555166	430.75174	0	
21835	30642.99107	0	18.3487969	427.6674899	0	
21307.5	29878.9131	0	21.95889619	424.5832398	0	
20780	29521.88438	0	9.04036212	421.4989897	0	
20252.5	29298.23846	0	4.241337233	418.4147396	0	
19725	29923.93297	0	13.4286951	415.3304895	0	
19197.5	29800.83865	0	31.53339836	412.2462394	0	
18670	30611.46593	0	11.09096982	409.1619893	0	
18142.5	29874.62872	0	43.45113697	406.0777392	0	
17615	30024.54662	0	1.907279679	402.9934891	0	
17087.5	30075.88315	5.878798813	10.39540681	399.909239	0	
16560	29437.2229	0.013607419	37.58492867	396.8249889	0	
16032.5	29935.48554	3.42128E-08	93.43828038	393.7407388	0	
15505	29613.7771	27.17029696	4.555632561	370.4814887	0	
14977.5	30365.1793	3.44194E-09	104.6582286	387.5722386	0	
14450	29964.97577	0.214760034	25.5217732	384.4879885	0	
13922.5	29563.81673	29.61863308	5.020411727	321.7037384	0	
13395	30204.31995	48.07573342	1.318592583	301.1444883	0	
12867.5	30423.60997	23.56856811	4.786472717	278.4352382	1	

Figure 21. Data Output from Multiple Simulation Runs

DP1	1000	0.9	22	188	-8.6	6.3	-7	-5	300	17500
Statistics	Mean	0.9	Standard Dev	0.307793506	95% Upper	1.03489645	95% Lower	0.765103548	# of Runs	20
DP2	953	10	7	376	-4.6	1.9	-8	-3	273	11500
Statistics	Mean	0.65	Standard Dev	0.489360485	95% Upper	0.86447169	95% Lower	0.435528311	# of Runs	20

Figure 22. Example of Statistical Output on the "DOE" tab

When the user clicks one of the simulator buttons shown in Figure 18, the simulator prompts the user for the radar transmitter power. A triangular distribution represents the radar transmitter power centered on the user's input. For the purposes of this thesis, the author used the Castor 2 J/C peak power of 30,000 watts with the minimum and maximum bounds being 29,000 and 31,000 watts respectively. Currently, the simulator is hard-coded to bound the minimum and maximum values at plus or minus 1,000 watts, but this could be changed in a future release. A normal distribution represents both the radar transmitter and missile receiver losses with a mean of -3 dB and a standard deviation of 1 dB. The missile noise factor is also normally distributed and has a mean of 6 and a standard deviation of 2. These values are also hard-coded, but could be changed in a future release of CEADS

An aircraft that exhibits Swerling Case I/II characteristics best represents the RCS fluctuations with an exponential probability density function. The author integrated the

exponential probability density function provided by Harney (2013a) to achieve a cumulative density function given by Equation 21. The simulator inserts a random number from 0 to 1 in place of CDF to determine the corresponding RCS (σ). When the user clicks one of the simulator buttons shown in Figure 18, CEADS prompts the user for the aircraft average RCS. For the purpose of this thesis, the author assumes the average radar cross section (σ_{av}) to be 24 dBsm as previously calculated in III.E. Figure 23 shows the inputs requested by CEADS from the user.

$$CDF = 1 - e^{-\frac{\sigma}{\sigma_{av}}} \tag{21}$$

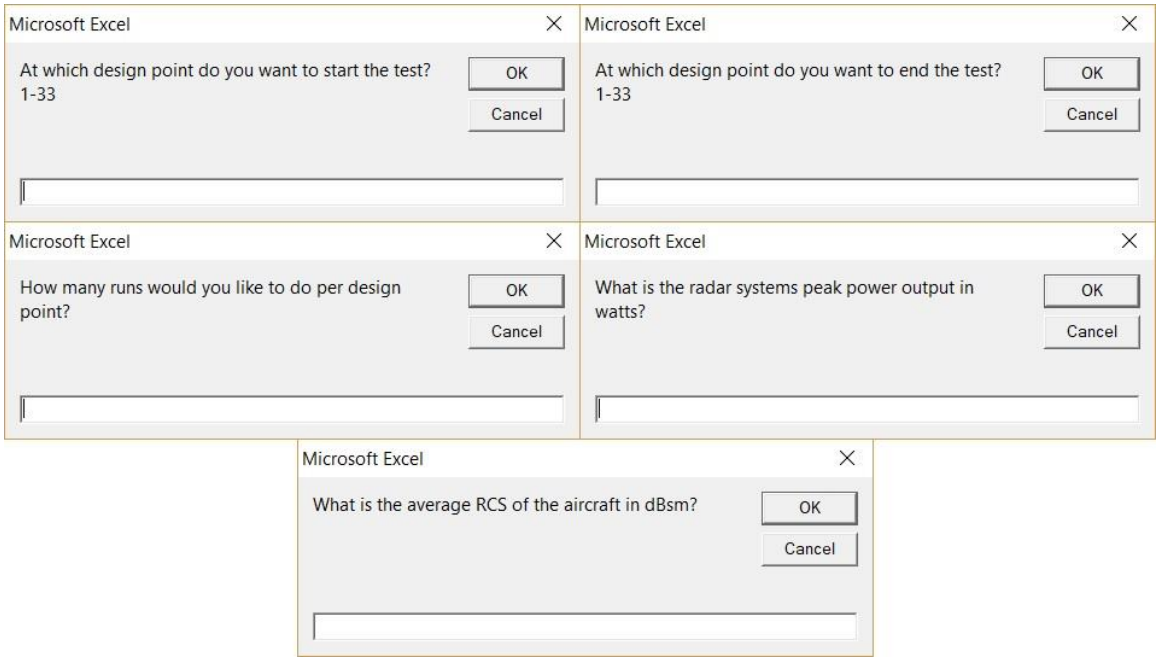

Figure 23. Inputs Requested by the Simulator for Multiple Runs

THIS PAGE INTENTIONALLY LEFT BLANK

V. SIMULATION EXPERIMENTS AND ANALYSIS

This chapter discusses the results of multiple simulation runs, performs a sensitivity analysis, and conducts a regression analysis of the data to determine the performance parameters of interest that are statistically relevant to the success rate of the EAD. CEADS uses the NOLH DOE to test many possible combinations of the EAD design space against an individual radar and missile system. This allows for analysis of the data in order to determine the best combination of performance parameters that maximizes the EAD effectiveness against a particular threat. Testing the CEADS against the Castor 2J/C radar provides a realistic scenario for the simulator and demonstrates its potential utility. Beyond the scope of this thesis, CEADS allows for data collection for a multitude of threat systems, analysis of data, and aides in developing high-level system requirements.

A. SIMULATION SETUP

The variables chosen as parameters of interest for the NOLH include jammer transmitter power, jammer transmitter loss factor, jammer gain, jammer bandwidth, EAD initial vertical and horizontal acceleration, EAD initial vertical and horizontal velocity, EAD deployment altitude, and EAD deployment range. The author's experience leads him to believe that the factors with the greatest effect on outcome are jammer transmitter power and gain. Therefore, the author began with a sensitivity analysis to explore how the jammer transmitter power and gain ranges affect the success rate of the EAD. The author kept the upper and lower bounds of all other variables the same in subsequent DOEs of the sensitivity analysis.

For the purpose of this thesis, the author completed 20 runs for each of the 33 total design points. The result of each run is either a "1" if the EAD succeeds in drawing the missile to an unfavorable engagement geometry or a "0" if the missile hits the target. The mean and sample standard deviation of all 20 runs is recorded on the DOE tab for each design point. The simulator uses this data to calculate a 95% confidence interval around the mean. If analysts desire a different interval width around an estimated mean, Equation

22 from Hayter (2014, 341) provides a way to calculate the necessary number of runs or replications.

$$number\_of\_runs = 4\left(\frac{t_{\alpha/2,n-1}s}{E}\right)^2 \tag{22}$$

B. SENSITIVITY ANALYSIS

The first DOE of the sensitivity analysis began with a minimum transmitter power of 1 watt and a maximum of 10 watts. The minimum gain was 1 dB and maximum of 10 dB. This DOE will be the baseline as the author assumes that range of values contains the minimum values for the EAD to achieve success. All following DOEs will stack the designs, meaning the power and gain ranges will change, but all other baseline variable ranges between DOEs. As an example, the baseline EAD loss factor range is from 1 to 10. All following DOEs will use this same range. According to Hernandez (2008), stacking NOLHs maintains the orthogonality of the overall design. Table 5 displays the results of the first DOE of the sensitivity analysis and an example of the statistical data output. The outcome shows that the design point exhibiting the greatest success rate is DP 33 with a power of 3 watts and gain of 5 dB resulting in 80% success.

Table 5. Statistical Data of Design of Experiments 1

Units	Watts	dB	dB	10 kHZ	m/s^2	m/s^2	m/s	m/s	m	m
low level	1	0	1	1	0	0	0	0	15	1000
high level	10	10	10	1000	-9.8	10	-10	-10	300	25000
decimals	0	1	0	0	1	1	0	0	0	0
factor name	Jammer Transmitter Power (P_J)	Jammer Transmitter Loss Factor (L_T)	Jammer Gain (G_J)	Jammer Bandwidth (B_J)	EAD Initial ↑ Accel	EAD Initial → Accel	EAD Initial ↑ Velocity	EAD Initial → Velocity	EAD Initial Deployment Altitude	EAD Deployment Range
DP1	10	0.9	5	188	-8.6	6.3	-7	-5	300	17500
Statistics	Mean	0.55	Standard Dev	0.510417786	95% Upper	0.773700458	95% Lower	0.326299542	# of Runs	20
DP2	9	10	2	376	-4.6	1.9	-8	-3	273	11500
Statistics	Mean	0.15	Standard Dev	0.366347549	95% Upper	0.310558892	95% Lower	-0.010558892	# of Runs	20
DP3	9	4.4	9	157	-0.3	5.9	-7	0	104	24250
Statistics	Mean	0.75	Standard Dev	0.444261658	95% Upper	0.944706256	95% Lower	0.555293744	# of Runs	20
DP4	6	8.8	10	407	-9.2	1.6	-8	-1	140	3250
Statistics	Mean	0.4	Standard Dev	0.50262469	95% Upper	0.620284983	95% Lower	0.179715017	# of Runs	20
DP5	9	0.3	5	220	-6.7	7.2	-4	-6	33	4000
Statistics	Mean	0.6	Standard Dev	0.50262469	95% Upper	0.820284983	95% Lower	0.379715017	# of Runs	20
DP6	10	9.4	4	282	-4.3	2.2	-2	-9	24	13750
Statistics	Mean	0	Standard Dev	0	95% Upper	0	95% Lower	0	# of Runs	20
DP7	7	4.7	10	251	0	6.6	-4	-9	264	1000
Statistics	Mean	0.55	Standard Dev	0.510417786	95% Upper	0.773700458	95% Lower	0.326299542	# of Runs	20
DP8	6	6.9	9	344	-8.9	2.5	-2	-10	166	23500
Statistics	Mean	0.55	Standard Dev	0.510417786	95% Upper	0.773700458	95% Lower	0.326299542	# of Runs	20
DP9	7	2.5	3	532	-7	3.1	0	-2	184	15250
Statistics	Mean	0.3	Standard Dev	0.470162346	95% Upper	0.506057733	95% Lower	0.093942267	# of Runs	20
DP10	8	6.6	4	688	-2.1	5.3	-1	-4	255	5500
Statistics	Mean	0.25	Standard Dev	0.444261658	95% Upper	0.444706256	95% Lower	0.055293744	# of Runs	20
DP11	7	2.2	8	969	-3.4	0.6	-1	-2	122	16000
Statistics	Mean	0.3	Standard Dev	0.470162346	95% Upper	0.506057733	95% Lower	0.093942267	# of Runs	20
DP12	8	7.2	7	938	-7.4	9.7	-5	-4	77	4750
Statistics	Mean	0.2	Standard Dev	0.410391341	95% Upper	0.379861935	95% Lower	0.020138065	# of Runs	20
DP13	6	1.6	3	563	-5.8	1.3	-10	-8	113	7750
Statistics	Mean	0.1	Standard Dev	0.307793506	95% Upper	0.234896452	95% Lower	-0.034896452	# of Runs	20
DP14	9	5.9	4	875	-1.5	5.6	-9	-7	86	19750
Statistics	Mean	0.15	Standard Dev	0.366347549	95% Upper	0.310558892	95% Lower	-0.010558892	# of Runs	20
DP15	7	1.9	9	906	-3.7	0	-7	-8	220	9250
Statistics	Mean	0.3	Standard Dev	0.470162346	95% Upper	0.506057733	95% Lower	0.093942267	# of Runs	20
DP16	8	6.3	6	1000	-8	9.1	-6	-7	247	19000
Statistics	Mean	0.05	Standard Dev	0.223606798	95% Upper	0.148	95% Lower	-0.048	# of Runs	20
DP17	6	5	6	501	-4.9	5	-5	-5	158	13000
Statistics	Mean	0.25	Standard Dev	0.444261658	95% Upper	0.444706256	95% Lower	0.055293744	# of Runs	20
DP18	1	9.1	6	813	-1.2	3.8	-3	-5	15	8500
Statistics	Mean	0	Standard Dev	0	95% Upper	0	95% Lower	0	# of Runs	20
DP19	2	0	9	625	-5.2	8.1	-3	-7	42	14500
Statistics	Mean	0	Standard Dev	0	95% Upper	0	95% Lower	0	# of Runs	20
DP20	2	5.6	2	844	-9.5	4.1	-3	-10	211	1750
Statistics	Mean	0	Standard Dev	0	95% Upper	0	95% Lower	0	# of Runs	20
DP21	5	1.3	1	594	-0.6	8.4	-2	-9	175	22750
Statistics	Mean	0.35	Standard Dev	0.489360485	95% Upper	0.564471689	95% Lower	0.135528311	# of Runs	20
DP22	2	9.7	6	781	-3.1	2.8	-6	-4	282	22000
Statistics	Mean	0	Standard Dev	0	95% Upper	0	95% Lower	0	# of Runs	20
DP23	1	0.6	7	719	-5.5	7.8	-8	-1	291	12250
Statistics	Mean	0.3	Standard Dev	0.470162346	95% Upper	0.506057733	95% Lower	0.093942267	# of Runs	20
DP24	4	5.3	1	750	-9.8	3.4	-6	-1	51	25000
Statistics	Mean	0	Standard Dev	0	95% Upper	0	95% Lower	0	# of Runs	20
DP25	5	3.1	2	657	-0.9	7.5	-8	0	149	2500
Statistics	Mean	0.15	Standard Dev	0.366347549	95% Upper	0.310558892	95% Lower	-0.010558892	# of Runs	20
DP26	4	7.5	8	469	-2.8	6.9	-10	-8	131	10750
Statistics	Mean	0.55	Standard Dev	0.510417786	95% Upper	0.773700458	95% Lower	0.326299542	# of Runs	20
DP27	3	3.4	7	313	-7.7	4.7	-9	-6	60	20500
Statistics	Mean	0	Standard Dev	0	95% Upper	0	95% Lower	0	# of Runs	20
DP28	4	7.8	3	32	-6.4	9.4	-9	-8	193	10000
Statistics	Mean	0.55	Standard Dev	0.510417786	95% Upper	0.773700458	95% Lower	0.326299542	# of Runs	20
DP29	3	2.8	4	63	-2.5	0.3	-5	-6	238	21250
Statistics	Mean	0.5	Standard Dev	0.512989176	95% Upper	0.724827419	95% Lower	0.275172581	# of Runs	20
DP30	5	8.4	8	438	-4	8.8	0	-2	202	18250
Statistics	Mean	0.3	Standard Dev	0.470162346	95% Upper	0.506057733	95% Lower	0.093942267	# of Runs	20
DP31	2	4.1	7	126	-8.3	4.4	-1	-3	229	6250
Statistics	Mean	0.4	Standard Dev	0.50262469	95% Upper	0.620284983	95% Lower	0.179715017	# of Runs	20
DP32	4	8.1	2	95	-6.1	10	-3	-3	95	16750
Statistics	Mean	0.05	Standard Dev	0.223606798	95% Upper	0.148	95% Lower	-0.048	# of Runs	20
DP33	3	3.8	5	1	-1.8	0.9	-4	-3	68	7000
Statistics	Mean	0.8	Standard Dev	0.410391341	95% Upper	0.979861935	95% Lower	0.620138065	# of Runs	20

The goal of the second and third DOEs of the sensitivity analysis was to determine the effect of increasing the EAD transmitter power on the success rate of the EAD. DOE 2 maintained the same minimum and maximum EAD gain, but increased the minimum power to 10 watts and maximum to 100 watts. DOE 3 also maintained a fixed gain, but the power range was from 100 to 500 watts. Again, the baseline DOE variables stack in DOE 2. Figure 24 shows a graphical composite of all DOE success rates based on power. Visually, one can determine that there is a clear correlation between increased power and

increased success rate. While DOE 1 has nearly 60% of all EAD configurations having less than 50% chance of success, DOE 3 where the range of power is from 100 to 500 watts, nearly 70% of the EAD configurations are above the 50% success rate.

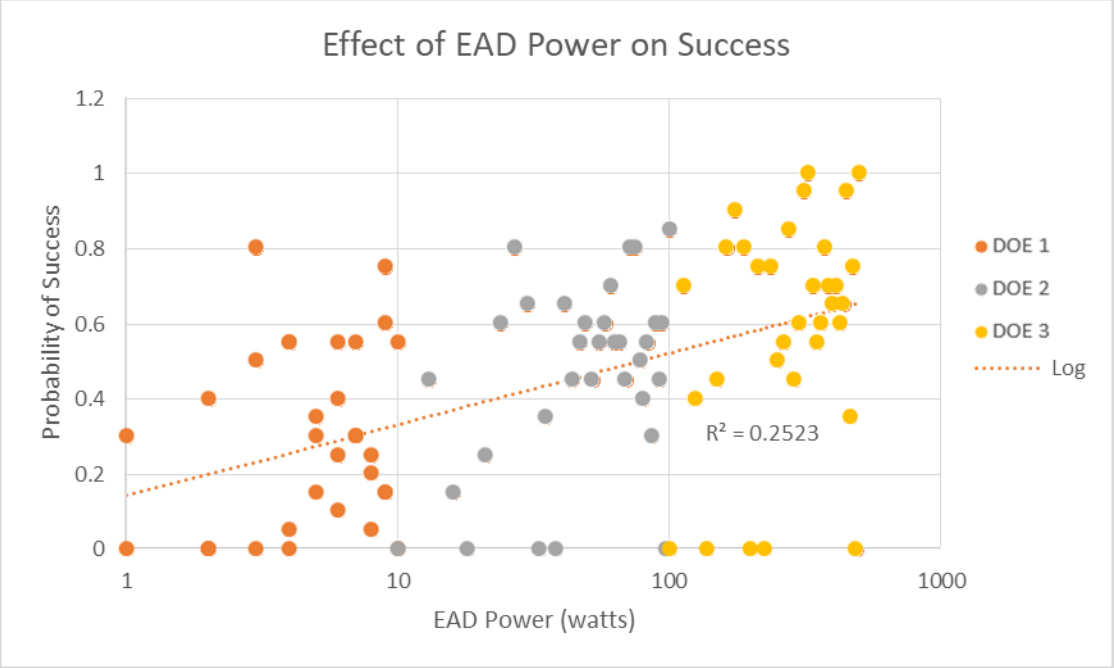

Figure 24. Effect of Decoy Power on the Probability of Success

Table 6 displays a few of the interesting results of DOE 2 of the sensitivity analysis. When compared to the results of the baseline DOE in Table 5, the results show that increasing power by approximately ten times can result in as much as a 50% increase in success, as demonstrated by DP 11 and DP 16. In another instance, DP 20 and 22, which previously had a 0% success rate, now have a 25% and 15% chance of success respectively. The average overall success rate of the baseline DOE is only 28.5%. DOE 2 has an average success rate of 46.1%.

Table 6. Noteworthy Results from Design of Experiments 2

DP11	75	
Statistics	Mean	0.8
DP16	83	
Statistics	Mean	0.55
DP20	21	
Statistics	Mean	0.25
DP22	16	
Statistics	Mean	0.15

Table 7 displays a few interesting results from DOE 3 of the sensitivity analysis. When compared to the results of the baseline DOE in Table 5, the results show that increasing power by approximately 50 times can result in as much as a 60% increase in success, as demonstrated by DP 4. DP 1, 3, and 4 has the highest success rates calculated thus far. DP 20, which had a 0% success rate in the baseline DOE, now has a 45% chance of success and DP 22 has a 40% probability of success.

When compared to DOE 2, nearly every design point saw an increase in probability of success from between 5% up to 40%. The average probability of success for DOE 3 is 58.9% compared to DOE 2 of 46.1% and the baseline DOE of 28.5%. DP 16, which experienced the greatest improvement in success between the baseline and DOE 2, only experienced an increase of 5% even though the power was increased by nearly 500%. This might indicate that further increasing power for these design points will have no further effect on the probability of success; there is a limit for increasing the probability of success by only increasing power. Another factor must be investigated to determine if probability of success can be further increased.

Table 7. Noteworthy Results from Design of Experiments 3

DP1	500	
Statistics	Mean	1
DP3	450	
Statistics	Mean	0.95
DP4	325	
Statistics	Mean	1
DP16	425	
Statistics	Mean	0.6
DP20	150	
Statistics	Mean	0.45
DP22	125	
Statistics	Mean	0.4

The goal of DOE 4 and 5 of the sensitivity analysis was to determine the effect that only increasing gain would have on the probability of success. EAD transmitter power resets to the baseline of 1 to 10 watts. DOE 5 used a gain range of 10 to 30 dB and DOE 6 used a range of 30 dB to 50 dB. All other variable ranges remained fixed. Figure 25 shows a graphical composite of all DOE success rates based on gain. Visually, one can determine that there is a clear correlation between increased gain and increased success rate. While DOE 1 has nearly 60% of all EAD configurations having less than 50% chance of success, DOE 5 where the range of gain is from 30 to 50 dB, nearly 85% of the EAD configurations are above the 50% success rate.

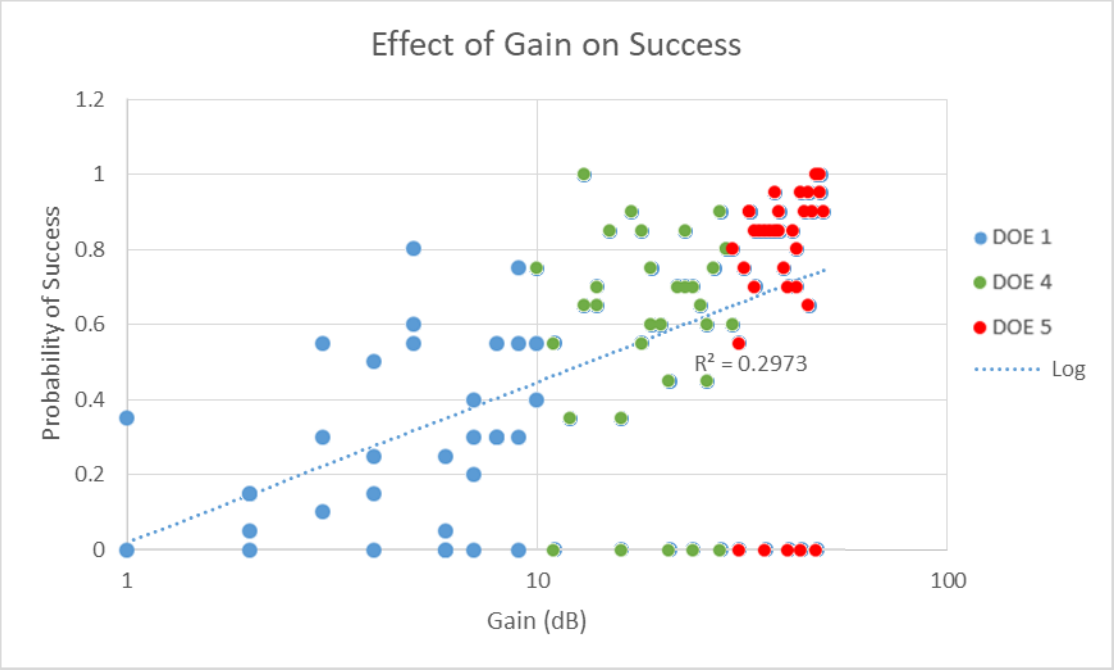

Figure 25. Effect of Decoy Gain on Probability of Success

Table 8 displays a few of the interesting results of DOE 4 of the sensitivity analysis. When compared to the results of the baseline DOE in Table 5, the results show that increasing gain from 2 dB to 13 dB can result in an impressive 85% increase in success, as demonstrated by DP 2, which achieved a 100% probability of success. DP 16 saw an increase from 5% to 70% when increasing gain by 16 dB. DP 20 and 22, which previously had a 0% success rate, now have a 35% and 45% chance of success respectively.

Table 8. Noteworthy Results from Design of Experiments 4

DP2	9	
Statistics	Mean	1
DP16	8	
Statistics	Mean	0.7
DP20	2	
Statistics	Mean	0.35
DP22	2	
Statistics	Mean	0.45

Table 9 displays a few of the interesting results from DOE 5 of the sensitivity analysis. When compared to the results of the baseline DOE in Table 5, the results show

that increasing the gain range to between 30 dB and 50 dB increases probability of success across all design points except for those with 0% probability. DP 25 is the lowest success rate at 55% while all other design points are greater than or equal to 70% probability of success. DP 20, which had a 0% success rate in the baseline DOE, now has a 75% chance of success and DP 22 has a 70% probability of success.

When compared to DOE 4, nearly every design point saw an increase in probability of success with 12 of the design points having 90% or greater probability of success. DP 3 and DP 8 achieved a 100% probability of success, which is an improvement over both DOEs. The average probability of success for DOE 5 is 71.3% compared to DOE 4 of 57.7% and the baseline DOE of 28.5%. It appears clear that increasing gain provides for greater probability of success across the entire range of design points when compared to only increasing power.

Table 9. Noteworthy Results from Design of Experiments 5

DP3	9	
Statistics	Mean	1
DP8	6	
Statistics	Mean	1
DP20	2	
Statistics	Mean	0.75
DP22	2	
Statistics	Mean	0.7
DP25	5	
Statistics	Mean	0.55

One thing that becomes clear from the sensitivity analysis is that, regardless of the EAD system characteristics, altitude and range, with regard to gain, have an effect on the success of the EAD. It is clear from the data that the design points with a low altitude deployment (< 60 m) and a long range from the missile experience failure 100% of the time. This is because the EAD does not have the altitude to drive the missile to an unfavorable geometry. Instead, the EAD descends on the surface with the target aircraft remaining within the missile's field of view. This allows time for the missile to reacquire the target. DP 5 demonstrates the only time when a low altitude deployment might succeed. This design point has a deployment altitude of 33 meters; however, the deployment range

from the missile is only 4000 meters. This allows the EAD to succeed in pulling the missile off the target aircraft prior to surface impact. This indicates that deployment tactics, techniques, and procedures can have an effect on the success of the EAD. A potential deployment technique might be for the pilot flying at low altitude to wait until the missile is closer before deploying the EAD.

C. REGRESSION ANALYSIS

Following the sensitivity analysis, the author performed regression analysis on the output from the simulation runs to determine which factors were statistically significant to EAD success or failure. Figure 26 displays the results of the regression analysis at the 0.10 significance level. Not all primary factors are statistically significant on their own; significant two-way interactions capture primary factors that must still be considered in the analysis. Notably, the two factors which were explored as the most likely candidates for having an effect on success are absent from the primary factors. However, their two-way interaction is statistically significant, which indicates that their primary effects must be considered in the overall design of the EAD. The two-way interaction between loss and horizontal acceleration has the greatest effect on EAD success. Examining each factor shows that they are both independently significant.

Loss factor is significant because it represents the percent of EAD power remaining after experiencing transmitter losses due to inefficiency. For example, a 3 dB loss factor represents approximately 50% of power remaining. Because the loss factor is logarithmic in nature, going from -2 dB to -3 dB represents going from 63% power remaining to 50% power remaining. This small change can have a big impact on jam-to-signal which depends on the loss factor. As such, the loss factor is a conduit for the effects of power, which may explain why power does not show as a significant primary factor. A systems engineer must examine this factor closely to determine how to make the energy transmission as efficient as possible to minimize the loss factor.

Horizontal acceleration is significant because it represents the change in velocity of the EAD after deployment. A high acceleration value represents a rapid deceleration of the EAD following deployment. According to Equation 9, the jam-to-signal ratio (J/S)

increases with the square of the receiver to target range (R_R). Therefore, the greater the range to the EAD, the higher the J/S will be. A higher acceleration value represents a rapid deceleration of the system. The system decelerates until it reaches a horizontal velocity of zero which maximizes its range from the missile with respect to time. This maintains a high J/S for a longer period, which results in a higher probability of success. This might suggest that a systems engineer find a way to slow the EAD down as fast as possible following deployment.

Similarly, vertical acceleration is the next most significant factor captured by the two-way interactions between it and horizontal acceleration and loss factor. Vertical acceleration is significant because it has a direct effect on both duration of engagement and how rapidly the missile can be pulled to an unfavorable geometry. Vertical acceleration affects the duration of the engagement by how quickly the EAD falls away from the aircraft. The faster it accelerates, the faster it falls, and the sooner it impacts the water. If this happens too quickly, and the aircraft is still in the missile's beam width, then the EAD fails. This becomes the focus of a systems engineering trade-off. If the EAD accelerates too quickly away from the aircraft, it could fail to draw the missile away before it impacts the water. If it accelerates too slowly, then the target remains in the missile's beam width and there is a chance that it could reacquire the target.

These significant factors are important attributes that must be incorporated in any design alternatives for a new EAD because they drive the capability requirements of the system. These are some, but not all, of the factors that engineers must consider to ensure a future EAD system is successful. Further analysis is required to determine the correct combination of factors that allow for maximum probability of success. Other considerations such as ability to produce power may limit factors such as maximum power output. Another trade-off may consider the requirement of a high-gain EAD needing to point its antenna directly at the threat and the problems associated with localization of said threat.

Model Summary

S	R-sq	R-sq(adj)	R-sq(pred)
0.154223	95.60%	93.63%	90.09%

Coefficients

Term	Coef	SE Coef	T-Value	P-Value
Loss	-93.4	21.5	-4.36	0.000
Bandwidth	0.587	0.142	4.13	0.000
VAccel	355.2	75.5	4.70	0.000
HAccel	275.9	57.9	4.76	0.000
VVel	-82.9	18.6	-4.47	0.000
HVel	-39.8	14.2	-2.80	0.006
Alt	-2.618	0.754	-3.47	0.001
Range	0.02568	0.00673	3.82	0.000
Power*Gain	0.000096	0.000037	2.59	0.011
Loss*Bandwidth	-0.1069	0.0241	-4.44	0.000
Loss*VAccel	-7.61	1.61	-4.72	0.000
Loss*HAccel	-11.11	2.23	-4.99	0.000
Loss*VVel	-9.18	2.00	-4.60	0.000
Loss*HVel	-6.87	1.49	-4.63	0.000
Loss*Range	0.00653	0.00143	4.57	0.000
Gain*Bandwidth	0.000006	0.000003	1.95	0.053
Gain*Alt	0.000033	0.000011	2.93	0.004
Bandwidth*VAccel	-0.0897	0.0191	-4.70	0.000
Bandwidth*HAccel	-0.0565	0.0124	-4.56	0.000
Bandwidth*VVel	0.01310	0.00604	2.17	0.032
Bandwidth*Alt	0.001896	0.000438	4.33	0.000
Bandwidth*Range	-0.000033	0.000009	-3.76	0.000
VAccel*HAccel	-8.06	1.71	-4.72	0.000
VAccel*VVel	16.51	3.59	4.60	0.000
VAccel*HVel	-13.20	3.19	-4.14	0.000
VAccel*Alt	-1.241	0.277	-4.48	0.000
VAccel*Range	-0.001526	0.000327	-4.67	0.000
HAccel*VVel	15.94	3.35	4.76	0.000
HAccel*HVel	1.522	0.402	3.78	0.000
HAccel*Alt	-0.1010	0.0230	-4.40	0.000
HAccel*Range	-0.00987	0.00221	-4.47	0.000
VVel*Alt	0.782	0.169	4.63	0.000

Figure 26. Regression Analysis Results

The data that resulted from the sensitivity analysis demonstrates that CEADS produces statistically relevant results. The author collected the results of the sensitivity analysis and sorted them to show which combinations of variables produced the highest probability of success. Table 10 shows those design points that achieved a probability of success of 90% or greater. The data shows that either a low power setting with a high gain, or a high power with a low gain, is necessary to achieve high probability of success. Notably none of the designs with power in the 10 – 100-watt range succeeded in achieving a probability of success of 90%.

DP 3 had the most instances of high probability of success achieving 90% or greater in three out of the five DOEs. It seems to be a prime candidate for consideration of the EAD capability requirements. It demonstrates that an EAD with a power of less than 10 watts can still achieve success when coupled with a gain of 28 dB or greater. If power is increased to 450 watts then a gain of 9 dB will suffice. Additional reasons the EAD was able to succeed may be deduced from those factors that were identified as the major drivers during regression analysis. DP 3 has a loss factor of 4.4, which equates to 36% power remaining. This indicates that only 3.25 watts of power are transmitted, which seems low and would negatively affect the probability of success. However, the horizontal acceleration value is rather high which indicates rapid deceleration and works in favor of increasing probability of success. This rapid deceleration, coupled with zero horizontal velocity added at deployment, and a deployment range of 24,500 meters, combine to improve the jam-to-signal ratio. Lastly, the low vertical acceleration coupled with the long range and 104-meter high deployment work in favor of the EAD. Their combination provides enough time to draw the missile off the target. These results will be crucial to the development of system level requirements for a future EAD.

Table 10. Design Points with Greater than 90% Probability of Success

	Decoy Power	Loss Factor	Decoy Gain	Decoy Bandwidth	Vert Accel	Horiz Accel	Vert Vel	Horiz Vel	Altitude	Range	Success
DP 2	9	10	13	376	-4.6	1.9	-8	-3	273	11500	**1**
DP 3	9	4.4	48	157	-0.3	5.9	-7	0	104	24250	**1**
DP 8	6	6.9	49	344	-8.9	2.5	-2	-10	166	23500	**1**
DP 1	500	0.9	5	188	-8.6	6.3	-7	-5	300	17500	**1**
DP 4	325	8.8	10	407	-9.2	1.6	-8	-1	140	3250	**1**
DP 7	7	4.7	49	251	0	6.6	-4	-9	264	1000	**0.95**
DP 23	1	0.6	44	719	-5.5	7.8	-8	-1	291	12250	**0.95**
DP 26	4	7.5	46	469	-2.8	6.9	-10	-8	131	10750	**0.95**
DP 33	3	3.8	38	1	-1.8	0.9	-4	-3	68	7000	**0.95**
DP 3	450	4.4	9	157	-0.3	5.9	-7	0	104	24250	**0.95**
DP 8	313	6.9	9	344	-8.9	2.5	-2	-10	166	23500	**0.95**
DP 3	9	4.4	28	157	-0.3	5.9	-7	0	104	24250	**0.9**
DP 29	3	2.8	17	63	-2.5	0.3	-5	-6	238	21250	**0.9**
DP 2	9	10	33	376	-4.6	1.9	-8	-3	273	11500	**0.9**
DP 4	6	8.8	50	407	-9.2	1.6	-8	-1	140	3250	**0.9**
DP 5	9	0.3	39	220	-6.7	7.2	-4	-6	33	4000	**0.9**
DP 11	7	2.2	45	969	-3.4	0.6	-1	-2	122	16000	**0.9**
DP 15	7	1.9	47	906	-3.7	0	-7	-8	220	9250	**0.9**
DP 32	4	8.1	33	95	-6.1	10	-3	-3	95	16750	**0.9**
DP 33	175	3.8	5	1	-1.8	0.9	-4	-3	68	7000	**0.9**

VI. CONCLUSION AND RECOMMENDATIONS

A. CONCLUSIONS

From the results of the analysis, the author recommends that all significant factors be explored in a tradeoff analysis to determine the combination that results in the highest probability of success against all threat systems. The focus of design should be on a combination of high power, low loss factor, high gain, low bandwidth, medium vertical acceleration and velocity, high horizontal acceleration (deceleration), zero horizontal velocity, early deployment, and medium to high altitude.

J/S is linearly dependent on most of the aforementioned factors. As noted by the sensitivity analysis, producing either high power or high gain will increase the J/S produced by the EAD. The author did not examine generating both simultaneously, but the results of the sensitivity analysis prove that having both high power and high gain is not required for high probability of success. A tradeoff exists here as previously mentioned. High power production requires enough battery power to generate the necessary wattage. A large battery will take up space in an already space-constrained system. This could be overcome by using a smaller battery with greater energy density. Similarly, a large gain will require that the EAD be able to geo-locate the threat and point its main antenna in the threat's direction. This adds complexity to the design of the system. Therefore, systems engineers must consider the tradeoff between generating higher power outputs using batteries that take up more space, or the engineering difficulty of designing the system to leverage high gain by geo-locating the threat. Doing both simultaneously will cost more time and money with no added benefit.

High horizontal acceleration and zero horizontal velocity on deployment will ensure that the EAD creates a large miss distance by ensuring the EAD remains at the maximum engagement distance at which it was deployed. This allows the aircraft to fly out of the radar resolution cell while the threat remains focused on the EAD creating a large miss distance. This capability requirement could manifest in the design of the dispenser, which could deploy the EAD directly perpendicular to the flight path of the aircraft;

ensuring zero added horizontal velocity on deployment. Some form of drag device such as a parachute, streamer, or drag fins could then be used to ensure a rapid deceleration.

Lastly, the author concludes that one of two deployment schema should be considered. The first is a medium-to-high altitude engagement with an early deployment of the EAD at long range. This serves to allow maximum time for the EAD to draw the missile away from the aircraft and leverages the positive effects of the square of the range term on J/S. Keeping in mind that a helicopter's flight profile is typically relegated to 300 meters or less, the sensitivity analysis determined that the design points with low altitude deployment usually resulted in a 0% probability of success. Those design points that succeeded with a low altitude deployment did so by waiting until the missile was closer before deploying. This allows the missile to be drawn away before the EAD impacts the water. By analyzing DP 5 and 33, which had a high level of success, the author concludes that when deploying the EAD at a low altitude (<70 meters), the operator should use a range to altitude ratio of 100 to 1. For example, DP 33 had a deployment altitude of 68 meters and a range of 7000 meters resulting in a high probability of success. Again, a tradeoff exists here as a system engineer could design the system with a low vertical velocity and acceleration, which would allow low altitude deployments at longer ranges. This has the beneficial effect of requiring only one deployment schema but further tradeoff analysis should be conducted to determine the effect on engagement outcomes.

B. RECOMMENDATIONS

The first recommendation is that subject matter experts at military organizations such as NAVAIR validate CEADS to ensure that the data provided is reasonable and that CEADS provides a sound MSBSE tool to aid in the development of the capability requirements of a future EAD system. Next, NAVAIR should use CEADS in the acquisition strategy for a new EAD system. The modeling and simulation based approach may be leveraged to save time and money and is the first step on the path to systems acquisition. Though the results obtained in Table 10 are for a single threat system, these design points may prove to be a launching point for future system design space exploration. The author recommends that the stakeholders at NAVAIR explore the combinations of

factors that produced the highest probability of success when researching new threat systems.

The author recommends that another student continue the research conducted by this thesis. There is further benefit in exploring the results against a multitude of threat systems so that a more complete picture may be obtained of the performance required of a new EAD system. This research could go on to include a cost-benefit analysis to determine the optimum combination of performance parameters values that achieve the greatest probability of success at the lowest cost.

The author recommends a few possible improvements to the simulator that would improve its ability to deliver relevant results. The first recommendation is to implement Doppler. CEADS only incorporates mono-pulse radar characteristics in the radar model. Incorporating Doppler will provide greater realism and allows for modeling more sophisticated threat systems. Incorporating other types of radar such as continuous wave may also be possible and would improve realism as well as allow for analysis against a wider range of threat systems. Another improvement could include modeling an active missile with its own onboard radar since CEADS currently only models semi-active missiles.

The next recommendation involves implementing a method for the aircraft to execute a maneuver following EAD deployment. In a real-world engagement, a maneuver often accompanies any kind of countermeasure deployment. These maneuvers are designed to reduce aircraft RCS and to exit the radar cell while the threat is focused on the countermeasure. The individual aspects of the maneuver such as rate of turn could be entered as a design point variable. This would not only have an effect on the outcome of the engagement but could drive system deployment doctrine as well. The author has already determined that a low altitude deployment at long range should be avoided.

The author also recommends implementing slant range into future releases of CEADS. In an effort to simplify the model, the author assumed that horizontal and slant range distances were roughly equal due to the low altitudes of the engagement. This may not prove true if exploring the effects at high altitude engagements.

Lastly, improving efficiency of the coding will help in improving the ability to collect large amounts of data. The author is by no means a coding expert and taught himself Microsoft Visual Basic coding while working on the thesis. The author assumes that his code is not as efficient as it could be. The author found that the ability to collect data was the choke point of the thesis. Running CEADS on a supercomputer or conducting parallel computing could also help with collecting data faster. Another recommendation to improve efficiency is to remove the radar and missile models completely and instead roll them all into the EAD tab. This would prevent much of the cross-linked computation that occurs and could speed up computation times.

This study will inform the aviation community's acquisition strategy for an improved EAD. Constantly improving radar technologies have limited the effectiveness of currently employed airborne countermeasures and could one day render LO technology obsolete. Additionally, the increasing ranges seen from recent threat systems now put non-fighter aircraft at risk of being detected and engaged far away from hostile environments. These facts, coupled with the massive improvements in battery energy density and miniaturization of electronics such as DRFM have made it possible to develop small, lightweight, and smart EADs that greatly improve the capabilities of today's aircraft to defend themselves. There is an opportunity to address this issue now. A countermeasure that is agile, adaptive, and intelligent, which is employable on all aircraft across all services, is necessary to ensure that the United States may continue to dominate hostile airspace around the world.

APPENDIX A. EQUATION VARIABLE DEFINITIONS

α	Atmospheric Attenuation Coefficient (m^{-1})
$\alpha + \beta$	Multipath Beam Width (radians)
ΔR	Radar Range Resolution (m)
ε	Efficiency of Matched Filter (%)
η_b	Hits per Scan (unitless)
θ_{GA}	Grazing Angle (radians)
θ_b	Azimuth Beam Width (deg)
θ_{BW}	Elevation Beam Width (radians)
$\dot{\theta}_s$	Scan Rate (deg/s)
λ	Wavelength (m)
σ	Radar Cross Section (m^2)
σ_{av}	Average Radar Cross Section (m^2)
σ_0	Mean Backscatter Coefficient ($dBsm/m^2$)
σ_{SC}	Sea Surface Clutter Radar Cross Section (m^2)
τ	Pulse Duration (s)
A	Target Voltage Return (volts)
A_R	Receiver Area (m^2)
a_x	Acceleration along x-axis (m/s^2)
a_y	Acceleration along x-axis (m/s^2)
B	Radar Bandwidth (Hz)
c	Speed of Light (m/s)
CNR	Carrier-to-noise Ratio (unitless or dB)
E	Statistical Margin of Error
F	Receiver Noise Factor (unitless)
f_p	frequency (Hz)
G_T	Transmitter Gain (unitless)
G_J	Jammer Gain (unitless)
H_R	Height of Receiver (m)
H_T	Height of Target (m)
J/S	Jam-to-signal Ratio (unitless)
k	Boltzmann's constant (J/K)
L_R	Receiver Loss Factors (%)
L_T	Transmitter Loss Factor (%)
P_D	Probability of Detection (unitless)
P_{fa}	Probability of False of Alarm (unitless)
P_R/P_0	Multipath Detection Ratio (unitless)
P_T	Transmitter power (watts)
R	Range (m)
R_0	Initial Range (m)
R_{DET}	Radar maximum Detection Range (m)
R_R	Receiver to Target Range (m)
R_T	Transmitter to Target Range (m)

s	Sample Standard Deviation
SLL	Side Lobe Level (%)
T	Electronics Temperature (K)
t	time (s)
$t_{\alpha/s,n-1}$	student-t distribution (unitless)
T_{fa}	Time Between False Alarm (s)
V	Voltage of Noise Return (volts)
$V0$	Root Mean Squared Noise Level ($(V/2)^{1/2}$)
V_x	Velocity along x-axis (m/s)
V_y	Velocity along y-axis (m/s)

APPENDIX B. MODELS

Calculate Radar CNR					
Radar Transmitter Power (P_T)	30,000	Watts	44.771	dB	
Radar Transmitter Loss Factor (L_T)	63%		-2	dB	
Radar Receiver Loss Factor (L_R)	63%		-2	dB	
Radar Transmitter Area (A_T)	0.5542	m^2	Radius (m)		0.42
Frequency (f)	16	GHz			
Wavelength (λ)	0.01875	meters			
Radar Gain (G_T)	19808.691		42.969	dB	
Radar Receiver Area (A_R)	0.5542	m^2	Radius (m)		0.42
Aircraft RCS (σ)	251.19	m^2	24	dBsm	
Boltzmann's Constant (k)	1.38E-23	J/K			
Temperature (T)	290	K			
Radar Receiver Bandwidth (B_R)	2.20E+05	Hz			
Radar Noise Factor (F)	6		3.981071706	dB	
Radar to Target Range (R_T)	30000	m			
Attenuation factor (α)	0				
CNR	48738.226		46.879	dB	
Pulses to Integrate (Detection of Signals in Noise eq. 10.18)					
Pulse Width (τ)	0.000002	s			
Pulse Repitition Frequency (f_p)	7200	pps			
Scan Rate (ω_m)	18	rpm			
Beam Azimuth (θ_b)	1.50	deg			
Beam Elevation (θ_e)	0.67	deg			
Hits per scan (η_b)	100				
Calculate Bandwidth of Matched Filter and P_{fa} (Detection of Signals in Noise eq. 10.17)					
Matched Filter Assumption (Bτ)	0.44	(See Table Below)			
Radar Receiver Bandwidth (B_R)	2.20E+05	Hz	0.2200	MHz	
Time Between False Alarms (T_{fa})	120	min			
False Alarm Probability (P_{fa})	6.31E-10				
Benefit from Integrating 100 pulses for Swerling Case I/II (Chart)					
24	dB				
CNR Needed to Detect Swerling Case I/II Target					
22.982	dB	Calculate CNR			
Calculated CNR	46.879	dB			
Sea Clutter CNR	25.101	dB			
Total CNR	70.879	dB			
Multipath a factor?	Yes				
Detected?:	Not Detected Multipath				

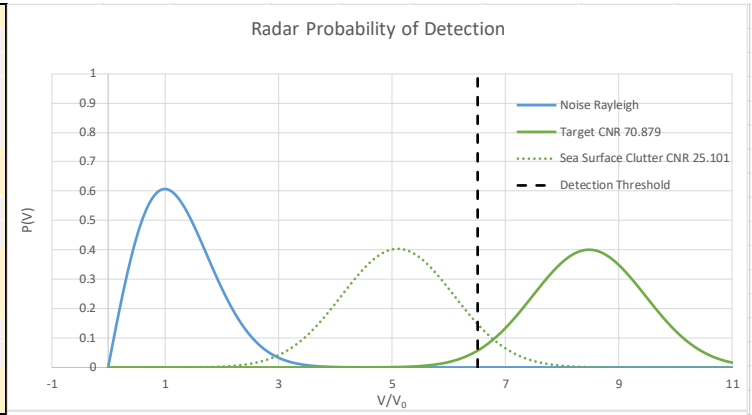

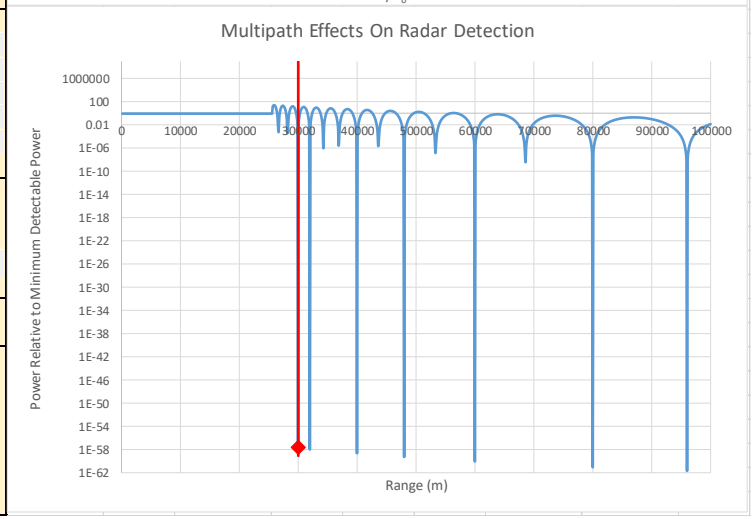

Figure 27. Radar Model

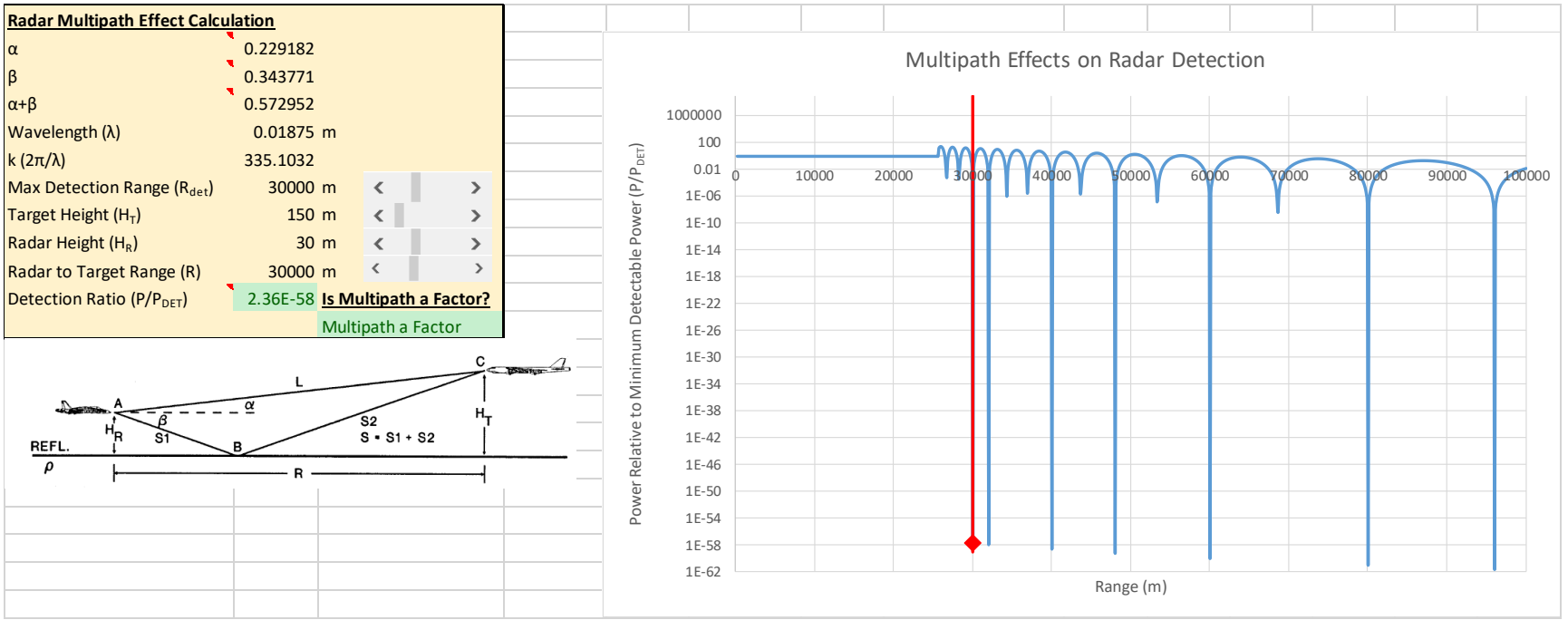

Figure 28. Multipath Model

System of Interest

PF	PD	PF	PD	PF	PD	PF	PD	PF	PD
6.31E-10	0.00	6.31E-10	0.00	1.00E-08	0.00	1.00E-10	0.00	1.00E-12	0.00
	0.00		0.00		0.00		0.00		0.00
	0.00		0.00		0.01		0.00		0.00
	0.01		0.01		0.02		0.01		0.00
	0.06		0.06		0.08		0.04		0.02
	0.15		0.15		0.19		0.12		0.08
	0.28		0.28		0.34		0.25		0.19
	0.44		0.44		0.49		0.41		0.35
	0.60		0.60		0.64		0.57		0.51
	0.72		0.72		0.75		0.70		0.65
	0.81		0.81		0.83		0.80		0.76
	0.88		0.88		0.89		0.87		0.84
	0.92		0.92		0.93		0.91		0.90
	0.95		0.95		0.95		0.94		0.93
	0.97		0.97		0.97		0.96		0.96
	0.98		0.98		0.98		0.98		0.97
	0.99		0.99		0.99		0.99		0.98
	0.99		0.99		0.99		0.99		0.99
	0.99		0.99		1.00		0.99		0.99
	1.00		1.00		1.00		1.00		1.00
	1.00		1.00		1.00		1.00		1.00

Calculate CNR for P_D	Calculate CNR for P_D	Calculate CNR for P_D	Calculate CNR for P_D	Calculate CNR for P_D
0.90	0.90	0.90	0.90	0.90
Calculated CNR	**Calculated CNR**	**Calculated CNR**	**Calculated CNR**	**Calculated CNR**
22.98151676	22.98151675	22.36784679	23.34752815	24.14690074

Calculate P_D for CNR		Calculate P_D for CNR		Calculate P_D for CNR		Calculate P_D for CNR		Calculate P_D for CNR	
CNR	P_D	CNR	P_D	CNR	P_D	CNR	P_D	CNR	P_D
23	0.90	23	0.90	23	0.91	23	0.89	23	0.87

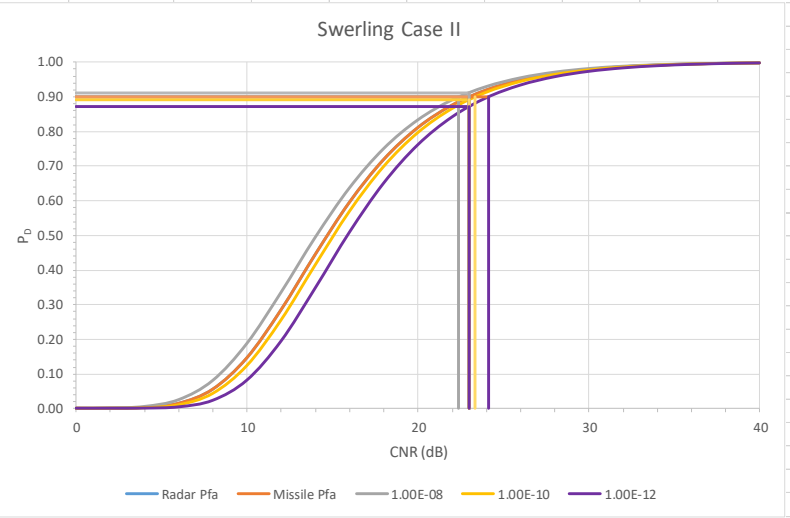

Figure 29. Swerling Case I/II Receiver Operating Characteristics

Radar Sea Surface Clutter				
Sea State/Radar Polarization	2H			
Target Height (H_T)	150	m		
Radar Height (H_R)	30	m		
Closest Radar Frequency	17	GHz		
Radar to Target Range (R)	30000	m		
Beam Elevation (θ_e)	0.011693706	rad		
Radar Range Resolution (ΔR)	300	m		
Grazing Angle	-0.105818104	deg		
Normalized Mean Sea Backscatter Coefficient (σ_0)	-48	$dBsm/m^2$		
σ	1.667994751	m^2	2.221947	dBsm
CNR_{SC}	323.6416442		25.10064	dB

Table 2-6. Definition of "sea state" used in sea clutter tables in this section.[1]

PEEBLES				CURRENT STANDARD		
"SEA STATE"	WIND SPEED knots	SIGNIFICANT WAVE HEIGHT feet	meters	SIGNIFICANT WAVE HEIGHT meters	WIND SPEED knots	"SEA STATE"
0	0	0	0	0	0	0
1	0 - 7	0 - 0.6	0 - 0.2	0 - 0.1	0 - 6	1
2	7 - 12	0.6 - 2.2	0.2 - 0.7	0.1 - 0.5	7 - 10	2
3	12 - 16	2.2 - 4.6	0.6 - 1.4	0.5 - 1.25	11-16	3
4	16 - 19	4.6 - 6.9	1.4 - 2.1	1.25 - 2.5	17 - 21	4
5	19 - 23	6.9 - 11	2.1 - 3.4	2.5 - 4.0	22 - 27	5
6	23 - 30	11 - 22	3.4 - 6.7	4.0 - 6.0	28 - 47	6

Normalized Mean Sea Backscatter Coefficient σ_0 for Grazing Angle of 0.1°				
	Reflection Coefficient in $dBsm/m^2$ for Given Frequency (Ghz)			
Sea State/Radar Polarization	3	5.6	9.3	17
0V	-	-	-	-
0H	-90	-87	-	-
1V	-80	-72	-65	-
1H	-80	-75	-71	-
2V	-75	-67	-56	-
2H	-75	-67	-59	-48
3V	-75	-60	-51	-
3H	-68	-69	-53	-
4V	-67	-58	-48	-
4H	-63	-60	-48	-
5V	-63	-55	-44	-
5H	-63	-58	-42	-
6V	-46	-	-	-
6H	-	-	-	-

Normalized Mean Sea Backscatter Coefficient σ_0 for Grazing Angle of 0.3°				
	Reflection Coefficient in $dBsm/m^2$ for Given Frequency (Ghz)			
Sea State	3	5.6	9.3	17
0V	-	-	-	-63
0H	-83	-79	-74	-
1V	-64	-60	-58	-54
1H	-74	-68	-66	-58
2V	-62	-55	-52	-52
2H	-66	-60	-56	-53
3V	-58	-50	-45	-47
3H	-60	-50	-46	-42
4V	-57	-	-43	-44
4H	-55	-	-42	-39
5V	-52	-	-39	-39
5H	-52	-44	-39	-38
6V	-	-	-34	-37
6H	-46	-	-34	-37

Figure 30. Sea Surface Clutter

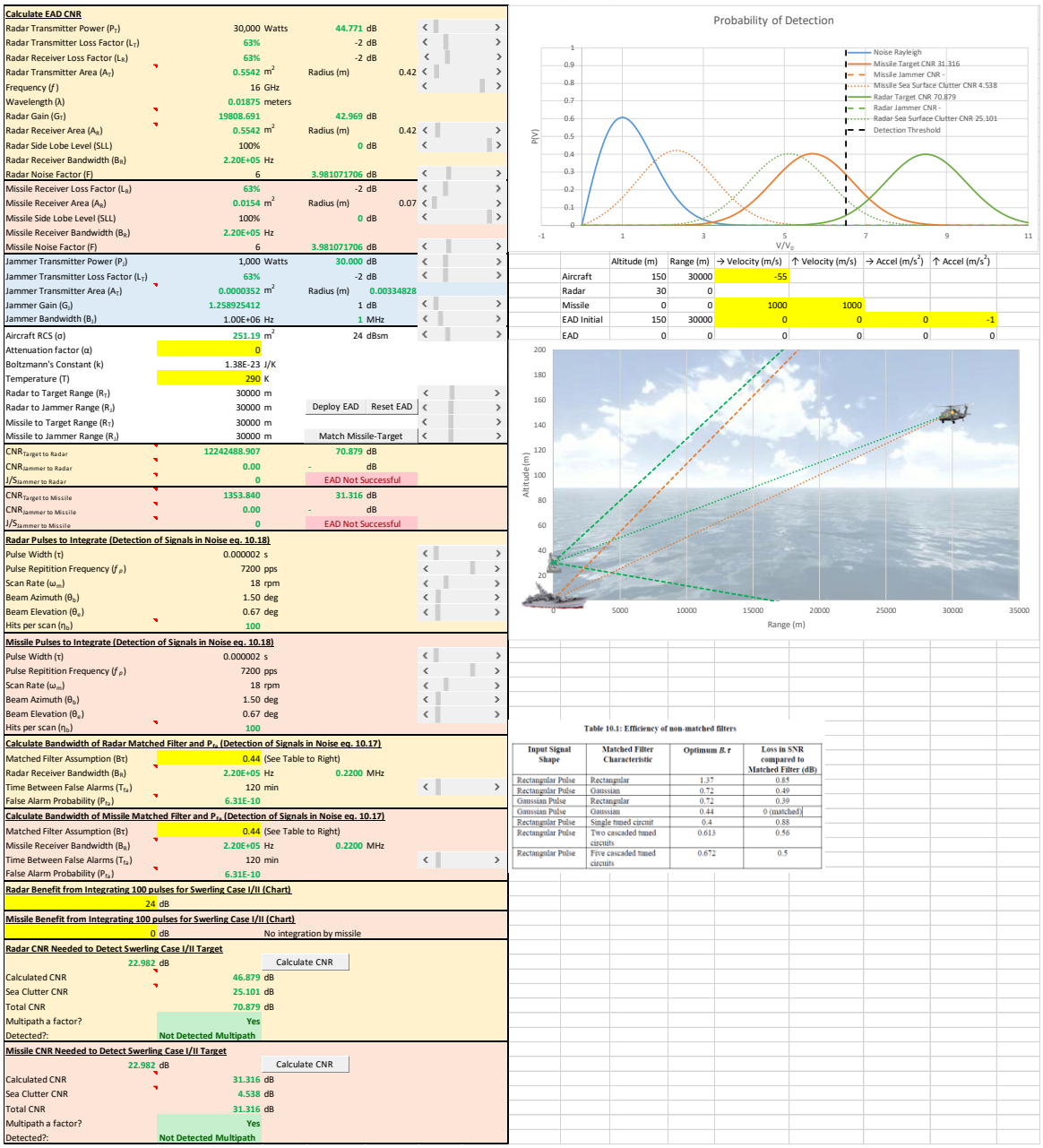

Figure 31. EAD Model

THIS PAGE INTENTIONALLY LEFT BLANK

LIST OF REFERENCES

Blanchard, Benjamin S., and Wolter J. Fabrycky. 2006. *Systems Engineering and Analysis*. 4th ed. Upper Saddle River, NJ: Prentice Hall.

Braud, Jeremy J. 2014. "Electronic Attack Platform Placement Optimization." Master's thesis, Naval Postgraduate School. https://calhoun.nps.edu/handle/10945/43881

Brooker, Graham. 2007. *Sensors and Signals*. Sydney: University of Sydney.

Chuter, Andrew. 2016. "RAF Considers BriteCloud to Counter Radar-Guided Missile Threat." *Defense News.* 30 March. Accessed 15 June 2017. http://www.defensenews.com/story/defense/international/europe/2016/03/30/raf-radar-guided-missile-threat/82417308/

Cioppa, Thomas M. 2002. "Efficient Nearly Orthogonal and Space-Filling Experimental Designs for High-Dimensional Complex Models." PhD Diss. Naval Postgraduate School. https://calhoun.nps.edu/handle/10945/9808

Defense Industry Daily. 2013. "Raytheon's ALE-50 "Little Buddy" Decoys." 25 April. Accessed 15 June 2017. http://www.defenseindustrydaily.com/raytheons-ale50-little-buddy-decoys-02573/

Eckstein, Megan. 2017. "NAVAIR Pushing Paperless Engineering to Speed Aircraft, Weapon Design." *U.S. Naval Institute News*. 24 October. Accessed 25 October 2017. https://news.usni.org/2017/10/24/navair-pushing-paperless-engineering-speed-aircraft-weapon-design

Gabriel, Dominguez. 2016. "What Is China's HQ-9 Air Defense System Capable of?" Interview by author 17 February. Accessed 28 September 2017. http://www.dw.com/en/what-is-chinas-hq-9-air-defense-system-capable-of/a-19053690

Gianni, Daniele, Andrea D'Ambrogio, and Andreas Tolk. 2015. *Modeling and simulation-based systems engineering handbook*. Boca Raton, LA: CRC Press.

Harney, Robert C. 2013a. *Sensor Signals and Functions*. Combat Systems Engineering. Vol. 1. Monterey: Naval Postgraduate School.

———. 2013b. *Sensor Technologies*. Combat Systems Engineering. Vol. 2. Monterey: Naval Postgraduate School.

———. 2013c. *Command and Control Elements*. Combat Systems Engineering. Vol. 5. Monterey: Naval Postgraduate School.

———. 2017. *Discussion on Radar Model Characteristics*, edited by Devon A. Cartwright.

Hayter, Anthony J. 2012. *Probability and Statistics for Engineers and Scientists*. 4th ed. Boston: Brooks/Cole.

Hernandez, Alejandro S. 2008. “Breaking Barriers to Design Dimensions in Nearly Orthogonal Latin Hypercubes.” PhD Diss. Naval Postgraduate School. https://calhoun.nps.edu/handle/10945/10306

Kopp, Carlo, Andrew Martin. 2012. “Type 345 HHQ-7 Naval Sino-Crotale engagement radar.” Digital Image. *Air Power Australia*. http://www.ausairpower.net/APA-HQ-7-Crotale.html#mozTocId698527

Koppenberger, Jim. 2017. “Navy EAD Plans and Programs (PMA-272).” Presentation at RF Summit #2, New Mexico State University, Las Cruces. 8 March.

Knott, E.F., D. J. Lewinski and S.D. Hunt. 1981. “Chaff Theoretical/Analytical Characterization and Validation Program.” Georgia Institute of Technology, Atlanta. 30 September. http://www.dtic.mil/dtic/tr/fulltext/u2/a105893.pdf

Kuzmin, Vitaly V. 2009. “Передатчик помех одноразового использования (Disposable jamming transmitter)” Accessed 25 March 2017. http://www.vitalykuzmin.net/Military/MAKS-2009/i-r9sbL7z/A

Mizokami, Kyle. 2016. “China Claims its New Anti-stealth Radars can Detect the F-22.” *Popular Mechanics*. 11 November. Accessed 10 September 2017. http://www.popularmechanics.com/military/weapons/a23846/china-anti-stealth-radars-detect-f-22/

Onnis, Gian Luca. 2012. “Towed Decoy Behind Typhoon.” Digital Image. *The Aviationist: David Cenciotti’s Weblog.* 16 April. Accessed 9 August 2017. https://theaviationist.com/2012/04/16/towed-decoy/

Payne, Craig M. 2010. *Principles of Naval Weapon Systems*. Second ed. Annapolis, Maryland: Naval Institute Press.

Rausch, Robert, David Benevelli, and Mort Serell. 2007. *Testing Programs for Transportation Management Systems: A Technical Handbook.* https://ops.fhwa.dot.gov/publications/tptms/handbook/index.htm

Streetly, Martin. 2005. *Jane's Radar and Electronic Warfare Systems 2005-2006*. Jane's Information Group Limited. pp. 160-161

Wikipedia, The Free Encyclopedia. 2008. "USNChaff." Digital Image. Accessed 15 May 2017, https://commons.wikimedia.org/wiki/File:Usnchaff.jpg

Yue, Tao. 2001. “Detection of the B-2 Stealth Bomber and a Brief History on ‘Stealth.’” *The Tech*. 30 November. Accessed 12 August 2017. http://tech.mit.edu/V121/N63/Stealth.63f.html

THIS PAGE INTENTIONALLY LEFT BLANK

INITIAL DISTRIBUTION LIST

1. Defense Technical Information Center
   Ft. Belvoir, Virginia

2. Dudley Knox Library
   Naval Postgraduate School
   Monterey, California